THE LONGITUDINAL EFFECTS OF PSEUDOPHOSPHORYLATED HUMAN TAU ON LOCUS COERULEUS FIBRE DENSITY IN TEMPORAL LOBE STRUCTURES AND ITS BEHAVIOURAL CONSEQUENCES IN MALE AND FEMALE RATS

By © Marie Ann Wasef

A Thesis submitted

to the School of Graduate Studies in partial fulfillment of the

requirements of the degree of

Master of Science, Department of Psychology, Faculty of Science

Memorial University of Newfoundland

February 2021

St. John's, Newfoundland and Labrador

Abstract

Abnormally phosphorylated tau is a protein commonly associated with Alzheimer disease (AD). Braak and Del Tredici (2011) have identified a noradrenergic nucleus, the locus coeruleus (LC), as the brain region to first express abnormal tau. Using a TH-Cre transgenic rat model of pretangle AD, we attempted to model the earliest prodromal stages seen in humans. We infused an adeno-associated virus (AAV) with a transgene coding a pseudophosphorylated human tau, htauE14, into the LC, and examined the behavioural consequences using four behavioural tests to assess memory, at 1-3 and 4-6 months post-infusion. Selective htauE14-GFP expression in LC neurons was confirmed using double immunolabelling for tyrosine hydroxylase and green fluorescent protein (GFP). We showed that >93% of LC neurons expressed GFP at 1-3 and 4-6 months post-infusion. Using an antibody against dopamine-β-hydroxylase, we showed higher relative optical density for LC-htauE14 infused rats at 1-3 months post-infusion in CA1 and the subgranular zone, suggesting htauE14-mediated changes in LC projections. Behavioural assays indicate subtle, sex-dependent impairment on hippocampal-dependent spatial memory. These results indicate that AAV-htauE14 is selectively expressed in LC neurons and can modify noradrenergic input to memory structures. Behavioural deficits may become more apparent if the LC-mediated projections are lost as animals age.

General Summary

Abnormally phosphorylated tau is a protein commonly associated with Alzheimer disease (AD). Braak and Del Tredici (2011) have identified a brain structure known as the locus coeruleus (LC) as the first brain region to express this abnormal protein. Using a rat model of early-stage AD, we examined the consequences of human tau on the behaviour and anatomy of these rats. We used a 4-test battery to assess memory conducted at two time points; we found that male AD rats were impaired on a test of spatial memory early in training. Additionally, using a technique known as immunohistochemistry, differences were observed between AD and control animals in the hippocampus, a brain region important for multiple types of learning and memory. These findings suggest that abnormal tau in the LC can contribute to anatomical and behavioural differences in our animal model of AD.

Acknowledgements

First and foremost, I would like to thank my supervisors, Dr. Darlene Skinner and Dr. Susan Walling, for their guidance and support throughout this project. I want to thank Dr. Skinner for her guidance and support over the past four years. Her mentorship and passion for research have had a tremendous impact on the scientist that I am today. I would also like to thank her for providing me with the opportunity to present at the world's biggest neuroscience conference twice during my time as a master's student; I will be forever grateful for those experiences. Not only has she been a tremendous support academically, but also on a personal level. I am beyond thankful for all the times she has taken time out of her busy schedule to support me and make me laugh. I would also like to thank Darlene for feeding and caring for our animals during the coronavirus pandemic. I want to thank Dr. Walling for her support and for passing on her expertise and wisdom in viral infusion surgeries, immunohistochemistry, and microscopy. Her passion for science and drive to conduct a project of such a magnitude inspired me to work hard and always ask questions. I am so appreciative. Sue also fed our animals during the pandemic, ran electrophysiology experiments, and collected brains for analysis. Her dedication to science is truly inspiring. I also want to thank her for her ongoing support during the past two years that my dad was ill. I am genuinely grateful for her compassion and support during his relapses; it meant the world. Thank you to Dr. Qi Yuan for being a member of my committee and for her advice throughout my project. I want to thank the summer research assistants, honours students, volunteers, and MUCEP workers who helped run behavioural tests, analyze data, and feed the animals.

Thank you to Dr. Ian Webb and Steve Milway for their support and incredible problem-solving skills. Although Steve retired at the start of my degree, his help during my undergraduate degree has made me the successful brain slicer and extractor I am today. I want to thank Ian for all the tips and tricks he has passed on, the most significant one being perfusions. Ian is also an incredible presence in the lab and genuinely cares about the students. I have enjoyed our chats about restaurants in the city and hearing about his experiences as a graduate student.

I cannot write this acknowledgment section without extending a huge thank you to Dr. Christina Thorpe. I always wonder if I would be where I am today if it was not for her. She kindly allowed me to volunteer in her lab in 2015 and hired me in the Summer of 2016. The opportunities that she has afforded me have allowed me to discover my passion for research. She trusted me to process tissue, and I will forever be grateful for her trust. Since then, she has provided me with several other opportunities. As a graduate student, she allowed me to be one of a few members of the department's Neuroscience Outreach Committee. I am genuinely grateful for this opportunity as it has allowed me to share my passion for science with individuals in the community from all age groups. Being able to give back to the community provided me with a sense of purpose and belonging. I am also appreciative of her concern with my personal life and for always checking-in to make sure that I was ok. I cannot thank you enough, Tina.

Thank you to the extraordinary animal care staff for taking such good care of our animals and braving snowstorms to feed our animals. I am so appreciative of them for making sure that I always had the supplies that I needed for surgery. Thank you to our wonderful veterinarian, Mary Timonin, for sharing her knowledge with me and taking the

time out of her busy schedule to care for our animals. Charlene Abbott has also been a tremendous help, and I appreciate all of her help with surgeries.

I would also like to thank the Natural Sciences and Engineering Research Council of Canada (NSERC), Aging Research Centre, the Department of Psychology, and the School of Graduate Studies for their financial support.

Last but not certainly not least, I would like to extend an enormous thank you to my family and friends. I want to thank my parents for their unconditional love and support. They have been there through it all, and I would not be where I am today if it was not for their confidence in me and for pushing me to be the best version of me. They never let me give up. I want to thank my brother, Philop, for being such a positive influence in my life. On the worst of days, just hearing his voice always made me feel better. He always knew how to cheer me up and always believed in me. I am fortunate to have such a loving and supportive brother, and I know I would not be the person I am today without him. I would like to thank Shannon, Chelsea, and Kayla for always being there. Their support, kindness, and friendship have been a vital part of my degree. Furthermore, their positivity, passion, and work ethic have inspired and motivated me to grow into the person I am today. They have been there through thick and thin, and I will forever be grateful for their love and support.

The biggest and most special thank you of all goes to my dad, Dr. Mourkus Wasef. While he will never be able to read this due to losing a long battle with multiple myeloma and renal failure in August 2020, I want to thank my dad for everything that he has done for me that has brought me to this point in my life. Even while he was sick, he was also concerned about my research and loved sending me research articles related to

Alzheimer disease. His love, support, and dedication meant so much to me, and I will be forever grateful. Dad, thank you for passing on your passion for science and life-long learning; these traits are a big part of who I am today. Thank you for everything you have done for me the past 24 years; I hope that this degree brings me one step closer to becoming the daughter you deserve and can be proud of. I will love you forever and dedicate this thesis to you.

Table of Contents

List of Figures

List of Tables

List of Abbreviations

Aβ	Amyloid beta
AD	Alzheimer disease
AP	Anterior-posterior
AVV	Adeno-associated virus
BFB	Blue fluorescent beads
CA1	Cornu ammonis 1
CA1 lac	Cornu ammonis 1 lacunosum moleculare
CA1 or	Cornu ammonis 1 oriens
CA1 pyr	Cornu ammonis 1 pyramidal
CA1 rad	Cornu ammonis 1 radiatum
CA3	Cornu ammonis 3 lacunosum moleculare
CA3	Cornu ammonis 3 lucidum
CA3	Cornu ammonis 3 oriens
CA3	Cornu ammonis 3 pyramidal
CA3	Cornu ammonis 3 radiatum
DA	Dopamine
DβH	Dopamine beta-hydroxylase
DβH-sap	Dopamine-β-hydroxylase IgG-saporin
DG	Dentate gyrus
DIO	Double-floxed inverted open
DSP4	N-(2-chloroethyl)-N-ethyl-2-bromobenzylamine
DV	Dorsal-ventral
EC	Entorhinal cortex
EPSP	Excitatory postsynaptic potential
FLEX	Flip-excision
GFP	Green fluorescent protein
GFP^+	Positively labelled for GFP
htau	Human tau
IgG-sap	IgG-saporin
IML	Inner molecular layer
LC	Locus coeruleus
L-DOPA	L-dihydroxyphenylalanine
lEC	Lateral entorhinal cortex
LPS	Lipopolysaccharide
mEC	Medial entorhinal cortex
ML	Medial-lateral
MML	Middle molecular layer

MWM	Morris water maze
NE	Norepinephrine
NE-LLP	Norepinephrine-induced long-lasting potentiation
NE-LTD	Norepinephrine-induced depression
NE-LTP	Norepinephrine-induced potentiation
NFT	Neurofibrillary tangles
NOR	Novel object recognition
OML	Outer molecular layer
ParaSub	Parasubiculum
p.i.	Post-infusion
PBS	Phosphate-buffered saline
PP	Perforant path
PreSub	Presubiculum
RAM	Radial arm maze
ROD	Relative optical density
SA	Spontaneous alternation
SGZ	Subgranular zone
TH	Tyrosine hydroxylase
TH^+	Positively labelled for TH
TH:Cre	Tyrosine hydroxylase cre-recombinase

The Longitudinal Effects of Pseudophosphorylated Human Tau on Locus Coeruleus Fibre Density in Temporal Lobe Structures and its Behavioural Consequences in Male and Female Rats

1. Introduction

1.1. Alzheimer Disease Overview

Alzheimer disease (AD), a progressive neurodegenerative disorder, is characterized by widespread brain atrophy and the deterioration of global cognitive functioning (Perry, 1999). It is the leading cause of dementia and typically affects individuals over the age of 65 but can also affect individuals as early as in their 30s (Iqbal et al., 1987; McKeever et al., 2018). With a growing ageing population, the projected impact of this disease on the healthcare system and economy has gained the attention of both researchers and policymakers (Kingston et al., 2018; Wu et al., 2016). With AD being a medical and global challenge, extensive research has been conducted to develop treatments to slow or halt the progression of the disease; however, to date, there are no such treatments available (Cummings & Fox, 2017). This failure is primarily due to the lack of understanding of the disease and where it originates (Cummings et al., 2014; Scheltens et al., 2016).

Alzheimer disease is caused by two hallmark neuropathological proteins: β-amyloid (Aβ) and abnormally phosphorylated tau (Bertram & Tanzi, 2005; Braak & Del Tredici, 2012; Sivanandam & Thakur, 2012). When amyloid precursor protein, a transmembrane protein found in neurons, is abnormally cleaved by enzymes in the cell, it forms Aβ (Scheltens et al., 2016). As a result of a combination of overproduction of this

protein and reduced clearance, these monomers begin to aggregate to their oligomeric form and may eventually form insoluble fibrils that become the foundation of plaques (Sengupta et al., 2016). These aggregates, known as amyloid plaques, accumulate extracellularly and disrupt the connections between neurons (Chow et al., 2010; Reiman, 2016).

Tau protein is found intracellularly and aids in stabilizing microtubules, the scaffolding of the cell (Brunden et al., 2010; Duka et al., 2013). In the normal human brain, there are two to three moles of phosphate per mole of tau. However, in the AD brain, this phosphate to tau ratio increases approximately three-fold so that the tau becomes hyperphosphorylated (Hu et al., 2002). Due to this abnormal increase in the number of attached phosphates, tau undergoes a conformational change and dissociates from the microtubule (Alonso et al., 2018). This dissociation of tau from the microtubules results in a degradation of the cell's scaffolding, affecting axonal transport (Kneynsberg et al., 2017). Furthermore, in its insoluble form, abnormal tau aggregates to form neurofibrillary tangles (NFT) intracellularly (Bancher et al., 1989). The presence of the tangles is cytotoxic as they interfere with various intracellular functions, resulting in the degeneration and eventual death of affected neurons (Busser et al., 1998).

Together, amyloid plaques and NFTs impair synaptic connectivity leading to the cognitive decline experienced by individuals with AD (Busser et al., 1998). While the neuropathology of AD can be characterized by the presence of amyloid plaques and NFTs, these two aggregates can also occur in individuals without dementia (Braak et al., 2006; Hyman et al., 2012). Hence, the presence of these proteins is not sufficient to diagnose an individual as having AD. In 1997, the National Institute on Aging and

Reagan Institute developed criteria for the neuropathological diagnosis of AD. One of the scales used in these criteria is the Braak 6-stage system.

1.2. Braak Staging of Tau and NFT in Alzheimer Disease

Braak and Braak (1991) examined the brains of 83 individuals, either with or without dementia, to characterize the progression of AD. They outlined six stages that described the distribution pattern of insoluble NFTs throughout the brain. Stages I and II are marked by the presence of NFTs in the transentorhinal region (see Figure 1D). In stages III and IV, the entorhinal cortex and temporal lobe regions, such as the hippocampus and amygdala, are affected (see Figure 1E). Furthermore, NFTs can be found in the subiculum, which receives its input from CA1 of the hippocampus and the entorhinal cortex. Finally, stages V and VI are defined by the presence of these tangles in higher-order association areas and the neocortex (see Figure 1F) (Braak & Braak, 1991; Canto et al., 2008).

In addition to these neurofibrillary stages, Braak and Del Tredici (2011) later outlined five pretangle stages in early AD-tauopathy in which abnormally phosphorylated tau is still in the soluble form, and symptoms of the disease are not present. These pretangle stages precede stages I to VI, which they described previously. In Stage *a*, pretangle material is first found in the processes of locus coeruleus (LC) cells (see Figure 1A-B) (Braak et al., 2011). In Stage *b*, this pretangle material moves to the soma and dendrites of LC cells (see Figure 1A-B). By Stage *c*, abnormal tau begins to infect other brainstem nuclei while remaining subcortical (see Figure 1A-B). At Stage 1*a*, abnormal tau, in its soluble form, can be found at the end of LC axon terminals ending in the transentorhinal cortex (see Figure 1C). In Stage 1*b*, the soma and processes of pyramidal

cells in the transentorhinal cortex fill with the pretangle material (see Figure 1C). From here, the spread can then be characterized by the aggregation of insoluble NFT outlined by stages I to VI mentioned above.

Braak et al. (2011) conducted a post-mortem analysis of over 2000 brains from individuals ages 1 to 100. They discovered that abnormal tau pathology is first detected in the LC, a noradrenergic nucleus found in the brainstem that supplies norepinephrine (NE) to the forebrain (Foote et al., 1983). Out of over 2000 individuals, only 10 were devoid of any detectable abnormal tau, with most of these individuals being younger than six years of age (Braak et al., 2011). Braak et al. (2011) identified the LC as the location where this abnormal pretangle material originates and that it spreads throughout the cortex from here in a systematic manner. Their analysis found that the severity of cognitive impairments experienced by patients correlated with their age and the stage of the disease, with those at higher stages being older and experiencing more severe impairments.

The discovery that the asymptomatic staging of pretangle material occurs decades prior to the onset of cognitive decline is of interest. Further exploration of this finding could lead to opportunities to halt or slow the aggregation of soluble tau to its insoluble form, NFTs. As such, developing a model that can accurately mimic Braak's pretangle stages would allow for the research of methods for early detection, intervention strategies, and biomedical treatment.

1.3. The Locus Coeruleus

The LC is a small noradrenergic brainstem nucleus with widespread projections to multiple areas of the forebrain and spinal cord, including the hippocampus, amygdala, olfactory bulbs, and raphe nucleus (Amaral & Sinnamon, 1977). The LC contains the

majority of noradrenergic neurons and is the primary source of NE throughout the CNS. The synthesis of NE involves several precursor chemicals and enzymes. First, the amino acid tyrosine is converted to L-dihydroxyphenylalanine (L-DOPA) by the enzyme tyrosine hydroxylase (TH) (Kvetnansky et al., 2009). Then, L-DOPA is converted to dopamine (DA) by the enzyme L-amino acid decarboxylase. Finally, DA is converted to NE by the enzyme dopamine beta-hydroxylase (DβH). While the synthesis of L-DOPA and DA occurs in the cell's cytosol, near the axon terminal, DA is transported into synaptic vesicles by a vesicular monoamine transporter. It is inside these synaptic vesicles where NE is synthesized. Finally, NE is released extracellularly primarily via synaptic varicosities (O'Donnell et al., 2012).

The LC has a significant role in mediating learning, memory consolidation, and attention (Amaral & Sinnamon, 1977; Aston-Jones et al., 1999) and is the sole source of NE to the hippocampus, neocortex, cerebellum, and some regions of the thalamus (Lindvall & Bjorklund, 1974). Studies have also shown that regions important in spatial learning, such as the prefrontal cortex and parietal cortices, receive extensive LC-NE projections (Benarroch, 2009). Studies have shown the LC-NE system to be negatively affected in neurodegenerative disorders such as Parkinson disease and Alzheimer disease (Del Tredici & Braak, 2013; Weinshenker, 2008). With extensive projections throughout the brain, dysfunction of the LC early on in the progression of sporadic preclinical AD is of interest.

This relationship between LC dysfunction and Alzheimer disease is not a novel finding. Tomlinson et al. (1981) reported a significant decrease in the number of LC

neurons in AD patients compared to controls. Before LC cell loss, the dysfunction of these cells has been reported prior to any observable AD-related symptomology (Braak et al., 2011). As such, LC neuron loss due to the aggregation of pretangle tau occurs during the later stages of the disease when NFTs are already present (Kelly et al., 2017). Not only is the LC implicated early on in the disease process, but it also continues to be involved during more advanced stages of the disease. Andrés-Benito et al. (2017) studied the brains of over 100 asymptomatic patients bearing NFT pathology at stages I-IV; they found that the LC is involved early with increasing numbers of pretangle positive cells with increasing age and stage of progression. Additionally, they noted mitochondrial impairment in cells that were positive for pretangle tau.

This accumulation of pretangle tau in LC neurons decades before the loss of these cells (Braak et al., 2011) suggests that a therapeutic window to slow or halt the progression of LC cell loss exists. To date, there is no treatment or disease-modifying intervention for AD (Cummings & Fox, 2017). Numerous clinical trials have failed to provide any therapeutic effects in mid- to late-stage AD due to the irreversible neuronal damage that has already occurred (Yiannopoulou et al., 2019). As such, research on methods for early detection and treatment is of interest.

1.4. The Hippocampal Formation

The hippocampal formation comprises the entorhinal cortex, dentate gyrus (Lethbridge et al.), subicular complex, and the three cornu ammonis fields, CA1, CA2 and CA3 (Blackstad & Flood, 1963). The hippocampal formation connectivity is largely unidirectional, with copious amounts of information entering via projections from the entorhinal cortex. The entorhinal cortex receives a vast amount of input from neocortical

association areas (Canto et al., 2008). The most widely described input into the hippocampus is the 'trisynaptic pathway.' The trisynaptic pathway originates in projections from the entorhinal cortex that form a bundle of fibres, known as the perforant path, which terminate at synapses with the granule cells of the DG (Hyman et al., 1986; Yeckel & Berger, 1990). From here, the axons of the granule cells project to CA3 via mossy fibres (Yeckel & Berger, 1990). In the CA3 subfield, the axons of CA3 pyramidal cells either project within this field reciprocally or project to CA1 via the Schaffer collaterals. Information is then projected back through the subicular complex to the deep layers of the EC.

1.5. Locus Coeruleus Projections to the Hippocampal Formation

The LC is the sole source of NE to the hippocampus, and hence, is critical to the normal functioning of the hippocampal circuitry (Ross et al., 2019). Through retrograde tracing methods using horse-radish peroxidase, it has been shown that hippocampal NE-containing afferents arise from cells of the dorsal LC (Mason & Fibiger, 1979). Large multipolar cells (Satoh et al., 1977) and fusiform cells (Mason & Fibiger, 1979) of the LC have been shown to project to the hippocampus. LC-NE efferents project to the dorsal and ventral hippocampus. Specifically, they have dense projections to the layers of the DG, with the density of innervation differing at each of the layers, with the majority innervating the hilus (Moore & Bloom, 1978; Swanson & Hartman, 1975). Regions CA3 and CA1 of the hippocampus have also been shown to receive LC-NE projections (Loughlin et al., 1986). When these LC-NE projections begin to disappear in patients with AD, deficits in memory, attention, and arousal begin to appear (Betts et al., 2019).

1.6. The Locus Coeruleus and Noradrenergic Modulation of Plasticity and Memory in Rodent Models

Neuman and Harley (1983) were the first to demonstrate that NE, directly applied to the PP-DG synapse in the hippocampus of anesthetized rats, produced an enduring β-adrenergic receptor-dependent potentiation of the evoked population response. This enduring facilitation of the PP-glutamatergic input on to DG granule cells was first coined 'norepinephrine-induced long-lasting potentiation' (or NE-LLP), but today is more commonly known as 'norepinephrine-induced potentiation' (or NE-LTP). Subsequently, this phenomenon was reproduced and more closely examined in hippocampal slice preparations where bath applied NE, or the β-adrenergic receptor isoproterenol, revealed a similar enduring potentiation of evoked activity at the PP-DG synapse (Dahl & Sarvey, 1989; Lacaille & Harley, 1985). In awake rats, Walling and Harley (2004) described an unusually delayed potentiation of the DG population spike and the synaptic field EPSP occurring 24-hours after glutamate-initiated NE release from LC neurons, an effect that was also blocked with the β-adrenergic receptor antagonist propranolol, and the protein synthesis blocker anisomycin. Interestingly, using electrical stimulation of LC neurons in awake rats to initiate endogenous NE release, Manahan-Vaughan and colleagues consistently report long-term depression (NE-LTD) at the PP-DG synapse, and modulation of PP frequency stimulation (Hansen & Manahan-Vaughan, 2015), and again at the CA3-Schaffer collateral input on CA1 pyramidal cell neurons (Lemon et al., 2009). Although these results seem contradictory, the bidirectional effects of NE-initiated release

events have contributed to the generation of the theory that glutamate amplifies NE effects (Mather et al., 2016).

NE-LTP is a phenomenon that occurs without tetanic (high frequency) stimulation to PP fibre input into the hippocampus and is dependent only on the stimulated release of NE from the LC (Brown et al., 2005; Quinlan et al., 2019; Walling & Harley, 2004; Walling et al., 2004), the activation of β-adrenergic receptors (Lethbridge et al., 2014), or natural behaviour that initiates release events from LC neurons, such as novelty detection (Kitchigina et al., 1997). Given that this naturalistic form of LTP can be produced in the hippocampus in animal models, it would be predicted that NE may modulate hippocampus-dependent memory in behaving animals. Indeed, LC-NE modulation of memory has been described in a variety of memory tasks in the normal rat. A non-exhaustive list of examples of LC-NE modulated memory includes: working memory (Kelly et al., 2019), spatial memory (Chalermpalanupap et al., 2018; Hou et al., 2019; Kelly et al., 2019), object recognition memory (Bharani et al., 2017).

Using a noradrenergic immunotoxin, dopamine-β-hydroxylase IgG-saporin (DβH−sap), Kelly et al. (2019) lesioned LC projection neurons to the prefrontal cortex in male and female Tg344-19 rats. Tg344-19 models of AD overexpress human amyloid-β precursor protein as a result of them possessing the Swedish APP mutation, *APP-swe,* and human presenilin-1 with the exon 9 mutation. These mutations result in an age-dependent increase in an accumulation of both soluble and insoluble amyloid plaques in the hippocampus and cortex. Furthermore, by 16-months of age, these animals develop tau pathology as seen by the presence of endogenous hyperphosphorylated tau and

argyrophilic tangles found in the hippocampus and cortex. Using the Barnes maze, they found that DβH−sap-lesioned animals spent significantly less time in the target quadrant during the probe trial and took significantly more time to locate the target hole than IgG-sap controls. Furthermore, DβH−sap-lesioned animals showed a greater number of revisits to previously explored holes in comparison to IgG-sap controls, suggesting impairments in working memory.

To explore the effects of LC-NE depletion on object recognition memory, Bharani et al. (2017) used the selective NE neurotoxin, N-(2-chloroethyl)-N-ethyl-2-bromobenzylamine (DSP4), to lesion the LC of Fischer 344 rats. In addition to this, animals also received injections of lipopolysaccharide (LPS) to produce cognitive changes secondary to neuroinflammation. Using the novel object recognition task, a discrimination index was used to calculate the amount of time spent exploring the novel object relative to the familiar object. These researchers found the DSP4-LPS rats performed worse on the NOR task compared to saline-injected and LPS-injected rats. These findings suggest that a reduction of NE to the hippocampus may have produced this cognitive deficit.

Recently, LC-NE has been implicated in difficult pattern separation, a phenomenon that identifies different or salient stimuli from the background, in a difficult olfactory discrimination task. Blockade of α- and β-adrenergic receptors in anterior piriform cortex decreased learning of the difficult odour discrimination task and the stability of neural representations measured by immediate early gene mRNA (Shakhawat et al., 2015). Given the role of the LC-NE in these memory processes and the

identification of the susceptibility of LC neurons to soluble and insoluble accumulation of abnormal tau, it is hypothesized that pretangle stage tau in LC neurons may identify susceptible individuals at the earliest AD stages by disruption of the LC-NE mediated memory tasks.

1.7. A Rat Model of Pretangle Stage Alzheimer Disease

Researchers at Memorial University have developed a rat model that parallels Braak's pretangle staging of AD. To our knowledge, there is no other comparable model of preclinical AD. To create our model, the LC of rats were infused bilaterally with an adeno-associated viral (AAV) vector carrying a transgene for pseudophosphorylated human tau (htauE14) protein (a gift from Karen Ashe, Addgene, MA, USA). Ghosh et al. (2019) found that the effects of this pseudophosphorylated htau modelled the progression of abnormal tau as described by Braak's pretangle staging. The gene was pseudophosphorylated at 14 out of 17 proline-directed disease-associated serine (S) and threonine (T) amino acid residues (T111, T153, T175, T181, S199, S202, T205, T212, T217, T231, S235, S396, S404, S422) to create tau that is persistently phosphorylated (Hoover et al., 2010). These 14 phosphorylation sites were substituted with glutamate to create pseudophosphorylated tau. To allow for the selective expression of htauE14 in the LC, a double inverted open reading frame (Galeano et al.) was used for TH:Cre-dependent expression.

To explore the influence of pretangle tau in the LC on behaviour and anatomy, we employed a preclinical rat model of AD, as described above. Ghosh et al. (2019) have previously shown that this model has compelling parallels to many of Braak's pretangle stages. Using simple and difficult versions of an odour discrimination task, Ghosh et al.

(2019) demonstrated that performance on both versions of this task was sensitive to the spread of pseudophosphorylated human tau protein that was infused bilaterally into the LC. In the simple version of the task, animals were required to discriminate between two distinct scents, such as orange extract and peppermint, to receive an appetitive reward. In the difficult version, animals were trained to discriminate between two similar odours, such as a 50:50 solution of 0.001% heptanol and 0.001% octanol and a 0.001% solution of heptanol.

In their first experiment, animals received AAV-htauE14 or AAV-GFP LC infusions at 2-3 months of age and were tested at approximately 5 months of age. These rats did not display impairments on either version of the odour discrimination task when compared to controls. In a second experiment, animals that received infusions at 2-3 months of age but then trained on the odour task at approximately 10 months of age were impaired on the difficult version of the task compared to rats in the control group but were not impaired on the simple version. Interestingly, in a third experiment, older animals that received infusions at 14-16 months of age were impaired on the difficult and the simple version of the task when tested at 20-22 months of age. Immunohistochemistry using DβH was used to analyze fibre density in piriform cortex, the primary olfactory cortex. Animals infused at 2-3 months, but tested at 10 months of age, and animals infused at 14-16 months of age had reduced LC fibre density in the piriform cortex in comparison to GFP- and non-infused controls. No differences were observed in animals that received infusions at 2-3 months of age but were tested at approximately 5 months of age. Furthermore, they found that this impairment in older animals (~20-22 months old)

correlated with a reduction in LC axonal density to the olfactory cortex, an overall reduction in the number of LC neurons, and a significant increase in the number of microglia in the piriform cortex.

These findings support the hypothesis that the presence of persistently phosphorylated tau in the LC serves as an initiation site for anatomical and cognitive changes in AD. Using this model and a battery of behavioural tests that assess for an AD phenotype would allow for the characterization of AD-associated cognitive decline and the spread of htauE14 from the LC to the EC and hippocampal complex. Impaired cognition and neuroanatomical changes in our model would support Braak's hypothesis that pretangles in the LC are, in fact, ground zero for AD pathology. As such, the current study used a more comprehensive battery of behavioural tests and a longitudinal approach to further understand the behavioural and neuroanatomical effects of LC-htauE14.

1.8. Study Overview

The purpose of the present study was to examine the behavioural and anatomical consequences of LC-htauE14 in both age- and sex-related contexts and provide a phenotypic profile for our rat model of pretangle AD. Two different groups were compared: htauE14 animals received bilateral infusions, directed at the LC, of a virus containing a gene that coded for pseudophosphorylated htau, and control animals received infusions of the same virus without the gene, infusions of vehicle with blue fluorescent beads (BFB), or were left unoperated. The cognitive functioning of these animals was assessed using a battery of behavioural tests including spontaneous alternation (SA), novel object recognition, Morris water maze (MWM), and a difficult radial arm maze (RAM) task. Furthermore, animals were tested during two time points at 1-3- and 4-6-

months post-LC-infusion (p.i.). After the completion of behavioural testing, brain tissue was collected for neuroanatomical analysis.

It was hypothesized that animals that expressed htauE14 in the LC would display progressive behavioural impairments compared to control rats on all four tasks and that these deficits would correlate with our hypothesized reorganization of LC projections to the temporal lobe memory systems.

2. Materials and Methods

2.1. Animals

Homozygous TH:Cre-KI Sprague-Dawley male rats (Sage Laboratories, MA, USA) were bred with wild-type Sprague-Dawley female rats (Charles Rivers Laboratories, QC, CA) to produce heterozygous TH:Cre-KI Sprague-Dawley offspring, to allow for the selective expression of htauE14 in the LC. The rats were singly housed in Green Line IVC Sealsafe Plus GR900 (Tecniplast, Buguggiate, Italy), and all cages contained corn cob bedding, Crink-l'Nest bedding, a PVC pipe tunnel, a wooden block, and a nylon dog bone. Their cages were kept in a temperature-controlled colony room (20°C), and they were maintained on a reverse 12:12 light/dark cycle (lights on at 1900). Animals were given *ad libitum* access to water and provided 75% of their adult *ad libitum* food consumption, described elsewhere (Hubert et al., 2000). Animals were maintained on this 25% restricted diet to increase survival rates and model healthy age-related weight changes.

All procedures for this experiment and animal housing were followed pursuant to the guidelines of the Canadian Council on Animal Care and were approved by the Memorial University of Newfoundland Institutional Committee on Animal Care.

2.2. AAV LC Infusions

At 3-months of age, rats in the experimental group received two 0.5 µl infusions of AAV2/9-rEF1a-DIO-EGFP-htauE14-WPRE, $2.05E^{+13}$vg/mL (Virovek, CA, USA), per hemisphere, and 0.2 µl of 0.05% blue fluorescent beads (BFB) directed at the LC. Blue fluorescent beads where used to localize infusion sites. Control animals received infusions of a similar virus that lacked the htauE14 transgene (AAV2/9-EF1a-FLEX-EGFP; $1.8E^{+13}$vg/mL; Laval Neurophotonics) and received two 0.5 µl infusions of the viral vector, per hemisphere, along with 0.2 µl of 0.05% BFB. Other control animals received just 0.2 µl of 0.05% BFB (0.1 µl per hemisphere), a sham operation but no infusion, or were left unoperated. All operated animals were anesthetized with isoflurane (induction at 3-5%, maintenance at 2-4%) and mounted on a standard stereotaxic apparatus (Model 900, Kopf, Tujunga, CA) in the skull-flat position. A scalp incision was made, and a single hole was drilled on either side of the sagittal suture using bregma as a reference (AP coordinates: -12.0-12.2 mm posterior to bregma; ML coordinates: ±1.3-1.4 mm lateral from the mid-line). Cannula placements were mapped according to the coordinates found in the Paxinos and Watson (2007) brain atlas. A 28-gauge stainless-steel internal cannula and a 22-gauge guide cannula (Plastics One Incorporated, VA, USA) were lowered at a 20° angle posterior to the vertical axis to avoid the transverse sinus, at a depth of 6.4-6.7 mm below brain surface. Infusions occurred at a rate of ~1.0 µl/min. Following surgery, animals were allowed one month to recover before the commencement of the behavioural battery.

2.3. Histology

2.3.1. Tissue Preparation

All rats were anesthetized with 15% urethane (1.5g/kg, i.p.) at a dose of 1mL/100g and perfused transcardially with 0.9% saline, immediately followed by 4% paraformaldehyde (PFA) in a phosphate buffer solution (PBS), pH 7.4. The brains were then extracted and stored overnight in 4% PFA in a refrigerator maintained at 4°C. The following morning, the brains were transferred to a 20% sucrose solution. Before sectioning, the brains were flash-frozen in 2-methylbutane stored at -40°C. The brainstem and cerebellum were then detached from the forebrain to be sectioned in different planes using a cryostat. The brainstem and cerebellum were sectioned in the coronal plane (30 μm), and the forebrain was sectioned in the horizontal plane. The fixed tissue was then stored in the cryoprotectant polyvinylpyrrolidone made in 0.1M PBS.

2.3.2. Immunohistochemistry

Brightfield. Sections were washed three times, 5 minutes per wash, in 0.1 M tris hydroxymethyl-amino methane (Tris buffer; pH 7.6). Next, sections were treated with 1% hydrogen peroxide in Tris buffer for 30 minutes. Sections were then rewashed in Tris buffer (three washes; 5 minutes per wash), followed by a 10-minute wash in Tris A (0.1% Triton X-100 in Tris buffer), and a 10-minute wash in Tris B (0.1% Triton X-100 and 0.005% bovine serum albumin (BSA) in Tris buffer). After this, the sections were then incubated in 10% normal horse serum (Vector Labs), made in Tris B, for 60 minutes. Following this incubation period, the sections were then washed for 10 minutes in Tris A, and then Tris B. Subsequently, the sections were incubated in a solution made in Tris B,

containing the primary antibody anti-DβH (mouse, Millipore) at a concentration of 1:10,000. The sections were left in the primary antibody for 48 hours on a rotator surrounded by ice packs (4°C). After two days, the sections were then washed for 10 minutes in Tris A and then Tris B. Following this, the sections were incubated in the secondary antibody biotinylated horse anti-mouse IgG (Vector Labs), made in Tris B, at a concentration of 1:400 for 60 minutes. Sections were then washed for 10 minutes in Tris A and then Tris D (0.1% Triton X-100 and 0.005% BSA in 0.5M Tris buffer). After these washes, the sections were incubated in avidin-biotin-horseradish peroxidase complex (ABC Elite Kit; Vector Labs) made in Tris D, at a concentration of 1:1000, for 2 hours. Again, sections were washed three times, 5 minutes per wash, in Tris buffer. Next, sections were transferred into diaminobenzidine and metal kit (ThermoFisher), were allowed to form for approximately 7 minutes to allow for visualization. Finally, the sections were washed three times, 5 minutes per wash, in Tris buffer before being mounted on gelatin-dipped microscope slides. The slides were allowed to air dry before they were dehydrated. The dehydration procedure consisted of seven steps, each lasting for 5 minutes. First, slides were immersed in 70% ethyl alcohol, then followed by 95% ethyl alcohol. Next, the slides were immersed in 100% ethyl alcohol twice and then twice in xylene. Immediately after the last step, the slides were coverslipped with Microkitt (Serum International, Montreal, QC). Sections were targeted for DβH to visualize NE-containing fibres.

Immunohistofluorescence. Free-floating sections for fluorescent antibody staining underwent a similar procedure as the sections used for brightfield microscopy.

The exceptions were that the sections were not treated using 1% hydrogen peroxide, Tris D, and different antibody pairs were used. To visualize TH, an enzyme found in NE-synthesizing neurons, the sections were treated with the primary antibody anti-TH (mouse, Millipore), at a concentration of 1:5000, and then the secondary antibody Alexa555 (donkey anti-mouse, ThermoFisher; 1:400). To visualize GFP, the sections were treated with the primary antibody anti-GFP (rabbit, ThermoFisher; 1:5000), and then the secondary antibody Alexa 488 (goat anti-rabbit, ThermoFisher; 1:400). Since aged animals were used in this study, TrueBlack Lipofuscin Autofluorescence Quencher (Biotium) was also used to reduce autofluorescence caused by lipofuscin, which can be found in the brains of ageing rats. Finally, sections were mounted onto gelatin-dipped slides and coverslipped using Vectashield with DAPI (Vector Labs).

2.3.3. Imaging

Brightfield images of DβH immunoreactivity in the hippocampus were collected using an Olympus BX51 confocal microscope (Richmond Hill, ON) and DP72 digital camera. Images were captured at a magnification of 4×, converted to grayscale, and later used for densitometry in various regions of the hippocampus. Fluorescence-labelled images were captured at a magnification of 20×.

2.3.4. Colocalization

We used colocalization to observe the spatial overlap of GFP and TH expression in the locus coeruleus. This is important for identifying LC-NE neurons and identifying which of those neurons successfully took up the virus and expressed GFP.

Fluorescent images revealing GFP and TH expression were overlaid using FIJI to examine the colocalization of GFP in TH-labelled LC cells. Numbers of total TH^+ and GFP^+ neurons were first counted in the LC of both hemispheres individually, followed by counts of TH^+/GFP^+ double labelled LC neurons, and summarized as the averaged measures per animal. Counts were conducted by three individuals blinded to the condition.

Data Analysis. For evaluation of TH^+ and GFP^+ co-expression in LC cells at 1-3 months p.i., analyses consisted of a one-way ANOVA with a between-subjects factor of group (htauE14, AAV-GFP, and control). Except where noted, Tukey's HSD post hoc test was used to analyze pairwise comparisons. At 4-6 months p.i., a two-tailed independent samples *t*-test was used to compare animals with htauE14 infusions and control conditions. Here and throughout, a value of $p < .05$ was considered to be significant.

2.3.5. Densitometry

All images were converted to 8-bit grayscale images using GNU Image Manipulation Program (GIMP; CA, USA). Densitometry was conducted using version 7.0 MCID Analysis software (MCID; UK) to calculate the relative optical density for a fixed number of samples per region of interest (see Table 1 for the pixel diameter for the cursor and the number of samples taken per region).

Data Analysis. For the evaluation of adjusted ROD values, sections were separated into a dorsal or ventral category. Anything above -5.6mm was considered dorsal, and anything at or below this coordinate was considered ventral. At each time

point, a two-tailed independent samples *t*-test was conducted for each region comparing the ROD values of htauE14 animals to controls.

2.4. Behavioural Tests

A 4-task battery of tests assessing working memory, recognition memory, spatial memory and pattern separation included the following: (1) spontaneous alteration; (2) a novel object recognition task; (3) the Morris water maze; and (4) a learned adjacent spatial arm separation task. This suite of tests was conducted twice within subjects, at 1-3- and 4-6 months post-infusion (p.i). Sex was a variable in the analyses of the spontaneous alteration task, novel object recognition task, and the Morris water maze task.

2.4.1. Spontaneous Alternation

To assess spatial working memory, animals were tested using the spontaneous alternation task described by Galeano et al. (2014). This task assesses spatial working memory as it is based on the idea that rats tend to explore the least recently visited arm. Therefore, for successful alternation, rats must know what arms they have visited most recently for efficient alternation.

Apparatus. The SA task was conducted using a black Plexiglas Y-maze with arms separated by 120° and measuring 16.5 cm wide × 48.8 cm long × 33.5 high. It contained blue Crayola™ Play sand, which was used for contrast during analysis using Ethovision XT (Noldus, VA, USA).

Procedure. Animals were placed in the center of the maze and were allowed 10 minutes to explore. At the end of each trial, the sand was mixed to control for scent tracking. The same procedure was used at 4-6 months p.i.

Data Analysis. The patterns of arm entries were recorded, and the series of triads for the first 8 minutes of the trial were counted, consistent with Galeano et al. (2014), using Ethovision XT. A triad was a sequence of visits into each of the three arms (1 → 2 → 3; 1→ 3 → 2; etc.). The arena was divided into four regions: start arm, novel arm, familiar arm and centre. The rat was considered to have entered an arm if its center point passed over an arm boundary that was set at 15 cm within the arm. The percentage of alternation was calculated as a ratio of the actual number of alternations to the total possible alternations that could have been made. The maximum number of alternations was calculated by subtracting two from the total number of arm entries. A two-way between-subjects ANOVA, with Sex (male, female) and Group (htauE14, control) as the between-subjects factors, was conducted. For all behavioural testing, Tukey's HSD post hoc test was used to analyze pairwise comparisons unless otherwise noted, and a value of $p < .05$ was considered significant.

2.4.2. Novel Object Recognition

Apparatus. To assess long-term recognition memory, animals were tested using the novel object recognition task. This task was conducted using the same black Plexiglas Y-maze described above for the SA task, and the SA test essentially served as the context habituation session 24-hours prior to NOR.

Procedure. Hippocampal-independent recognition memory was assessed using a two-trial recognition test, as described by Walling et al. (2016). All animals were habituated to the maze 24 hours prior to the exposure trial and were allowed to explore the maze for 10 min (SA test described above). During the exposure trial, two copies of an object were used, and one was placed in the same location in two arms, and the

remaining arm was the animal's start arm. The rat was placed in the start arm facing the wall to not bias it towards a particular arm and was allowed 15 minutes to explore the objects. Objects were cleaned with 70% ethanol, and the sand was mixed at the end of each trial to control for scent tracking. Three copies of the same object were used, but each was restricted to placement in one arm to avoid confounds that could occur if a previously explored object was in a new location during the test phase. Objects were made of non-absorbent materials, such as glass or plastic, so that they could easily be cleaned to control for scents. Objects included animal figures or decorative objects in the shape of pumpkins or fruits. Object sets were counterbalanced as Novel or Familiar within tests to control for possible preference effects for an object.

The test trial took place 24 hours after the exposure trial. During this trial, an object from the exposure trial was placed in one of the arms that were not the start arm (familiar object), and an object that the animal had not seen before was placed in the other arm (novel object). Again, the animal was placed in the same start arm used during the exposure trial, facing the wall, and was allowed 5 minutes to explore all three arms. The same procedure was used at 4-6 months p.i., but new objects were used at this time point.

Data Analysis. All three trials (habituation, exposure and test) were video-recorded and analyzed using Ethovision XT. The arena was divided into four regions: start arm, novel arm, familiar arm and centre. The test trial was analyzed, and the total time the rat spent in each arm was converted to a percentage of the total time in all three arms. The rat was considered to have entered an arm if its center point passed over an arm boundary that was set at 15 cm within the arm. An animal's first arm choice was also recorded. These data were analyzed using a three-way mixed ANOVA with Arm (Start,

Familiar, Novel) are the within-subjects factor, and Sex (male, female) and Group (htauE14, control) as the between-subjects factors.

2.4.3. Morris Water Maze

The Morris water maze (MWM) task is a test of spatial memory. In this version of the MWM, animals underwent three phases: cued, spatial, and probe (as described by Galeano et al., 2014). The same procedure was used at 4-6 months p.i.; however, the hidden platform was located in a different quadrant.

Apparatus. This task took place in a circular pool with a diameter of 176 cm and a depth of 91 cm. The pool was filled to a depth of 85 cm with approximately 2 cm of water covering the top of the platform. The escape platform was made of white plastic and was 10 cm in diameter and 83 cm high. The entire apparatus rested on a stainless-steel platform with wheels. The water was maintained at a temperature of 22 ± 1°C and made opaque using approximately 700 mL of non-toxic white tempera paint (Craftsmart, TX, USA). Four removable metal poles were attached to the side of the pool equidistant from each other, and curtain wire was used to drape black curtains for the cued phase of the test. During the hidden and probe phases, the poles remained attached to the pool; however, the curtain wire was removed.

Behavioural testing took place in a room (676 × 503 × 259 cm), which had windows lined in tin foil covering the north wall and doors located at the south and west walls. A black counter with cupboards below and a sink in the northeast corner lined the east wall. Additionally, along the east wall was a filing cabinet with a laptop where an experimenter stood and recorded data. Along the south wall was a table and wall

shelving, and on the west wall was a black and white striped poster. Finally, directly overhead was a piece of wood with a camera mounted on it, which rested where a ceiling tile belonged.

Procedure. During all three phases of the MWM task, animals were tested in dim lighting using four 60-Watt lamps. The pool was divided into four imaginary quadrants: northwest (NW), northeast (NE), southwest (SW), and southeast (SE). Each of the poles represented one of the four cardinal directions and served as the release points.

Cued. The cued phase occurred over two days, and animals were given four trials per day, with animals being released once from each cardinal point, with the order of release being randomized. Additionally, the platform was moved between trials, pseudorandomly, with each quadrant location used once per day. As previously mentioned, the pool was surrounded by black curtains to prevent access to external cues. Rats were trained to locate a hidden platform that was flagged using four orange and white fishing floats. Animals were put in the pool facing the pool wall to prevent biasing them in a particular direction and were given 60 seconds to find the platform before they were guided to the platform by the experimenter. Animals were given an intertrial interval of 10-15 minutes. After rats had located or were guided to the platform, they were left on the platform for 15 seconds before they were removed from the maze and returned to their holding cage.

Hidden. During this phase, the curtains were removed to allow access to extra-maze cues. Furthermore, the fishing floats were also removed from the platform. During this phase of testing, animals were given four trials per day for five consecutive days and were trained to swim to the platform, which remained static during this phase. The

platform was located in a quadrant 60 cm from the two closest poles, 38 cm from the pool wall, and 2 cm below the water surface. Again, release points were pseudorandomized between days, with each point being used once per day. A trial was complete once the animal had successfully located and climbed onto the platform, or if they were guided and placed on the platform by the experimenter after 60 seconds had passed. Again, animals were left on the platform for 15 seconds before they were returned to their holding cage, and they were given an intertrial interval of 5-10 minutes.

Probe. Twenty-four hours after the last Hidden trial, the platform was removed from the pool and rats were released from the quadrant directly opposite the quadrant that contained the platform during the Hidden phase. Rats were given 60 seconds to swim, and their behaviour was video recorded for later analysis.

Data Analysis. All three phases of this test were video recorded. The probe trial specifically was analyzed using Ethovision XT. The arena was divided into four equal quadrants, and time spent in the target quadrant was analyzed.

For the Cued phase, the data for each sex were analyzed using a three-way mixed ANOVA with Day and Trial as the within-subjects factors, and Group (htauE14, control) as the between-subjects factor.

For the Hidden phase, a four-way mixed ANOVA with Trial and Day as the within-subjects factors, and Sex (male, female) and Group as the between-subjects factors were used. When the assumption of sphericity was violated, the degrees of freedom were adjusted using the appropriate correction. Post hoc analyses were conducted using independent-samples *t*-tests.

Finally, for the Probe trial, a two-way ANOVA with Sex and Group as the between-subjects factors were used.

2.4.4. Radial Arm Maze

The radial arm maze task is a test of hippocampal-dependent memory (McDonald & White, 1995). One month prior to an animal's surgery date, animals were trained on the Separate version of the RAM task. In this variant, animals were trained to discriminate between two arm locations separated by 135°. This variant of the task is easier than the Adjacent version and was used to acquaint the rats with the task prior to behavioural testing one-month post-infusion. At 1-3- and 4-6 months post-infusion, animals were trained on the more difficult Adjacent version of the RAM task, which required them to discriminate between two arm locations separated by 45°.

Apparatus. Behavioural testing took place on an 8-arm maze constructed from black Plexiglas. The base of the maze was elevated 56 cm from the ground and rested on a stainless-steel base with wheels so that the maze could be easily manipulated. The center of the maze had a diameter of 28 cm, and the arms had a height of 28.5 cm and a width of 10 cm. The arms' walls were highest near the center of the maze and sloped downwards towards the end of the arm containing the food cup. Each arm contained a sliding door that was 10 cm wide, and 9 cm high used to restrict access to specific arms.

Pretraining and training for pre-operative and post-operative RAM took place in a room with dimensions 676 × 502 × 264 cm. This room contained a window covering the end of the west wall that was furthest from the sink, and a door located in the center of the east wall and another located at the end of the west wall, closest to the sink. A black

counter with shelves beneath and a sink in the southwest corner lined the south wall, and there was a table along both the east and west walls. The southwest corner of the room also contained a garbage can. The northwest corner had a filing cabinet and a small desk with a computer. Along the east wall directly in front of the maze was a table where the male rats' cages were kept. The cages of the female rats were kept on the black counter lining the south wall.

Procedure. During pretraining and training sessions, both pre- and post-infusion, animals were tested in dim lighting using two 60-watt lamps. Animals were food restricted the day prior to the start of pretraining to ensure that they were motivated to complete the task. Finally, novel reinforcers were used each time this procedure was conducted to prevent the animals from losing interest in a familiar food. Reinforcers that were used included Froot Loops, miniature chocolate chips, and chocolate Cheerios. The same post-infusion procedure was used at 4-6 months p.i.; however, the task was completed using different food and no-food arm locations.

Pretraining. Pretraining occurred over two consecutive days preceding the start of training. On each day, animals had access to two arms, the food arm and one no-food arm, while the remaining six arms were blocked. Both arms were baited along the entire length of each. On the second day of pretraining, the animal had access to the no-food arm blocked the previous day, while the second no-food arm was now blocked. During pretraining, animals were placed singly in the center of the maze facing a closed arm, as not to bias them towards a particular open arm and were given five minutes to explore the maze. After each pretraining session, two pieces of the reinforcer were placed in each animal's home cage to limit the effects of food neophobia on training.

Training. Twenty-four hours after the last pretraining session, the training phase began. During this phase, rats were trained to locate a piece of food from a food cup at the end of a reinforced arm that was not visible from the maze's surface. On each trial, access to six arms was blocked while only two remained open, a reinforced arm location and a non-reinforced arm location. Each animal was assigned a reinforced arm location and its two corresponding non-reinforced arm locations, one to the left and the other to the right of the reinforced arm. On any given trial, animals always had access to the reinforced arm; however, access to only one of the two non-reinforced arms was allowed. Access to the non-reinforced arms was pseudorandomized, with a particular arm not being open for more than two consecutive trials.

At the start of a trial, a rat was removed from its cage and carried towards the maze. It was then placed in the center of the maze facing one of the six closed arms; this was pseudorandom. Once on the maze, the rat was allowed 60 seconds to choose an arm. A choice was defined as the animal's nose passing a line located 33 cm inside the arm. If a rat chose the non-reinforced arm, it was removed from the maze and returned to its home cage. If the rat chose the reinforced arm, it was allowed to eat the food before it was removed from the maze and returned to its home cage. Animals were returned to their cage following the same path used to walk towards the maze to avoid path characteristics from serving as cues. Upon completion of a trial, rats were given 60 seconds in their home cage before the start of the next trial. During this time, the maze was rotated by at least 90° so that different arms were used to prevent the use of olfactory cues. Animals received ten trials per day for a maximum of 15 days. Animals were considered to have

learned the task if they reached a criterion of 8/10 trials correct. Once this criterion was achieved, the animal received no more trials.

Data Analysis. All data were recorded by hand and were analyzed using a two-way ANOVA with Sex and Group as the between-subjects factors.

3. Results

3.1. Colocalization of GFP$^+$ and TH$^+$ Neurons in Locus Coeruleus

Locus coeruleus neurons that were positively labelled for TH (TH$^+$) were assessed for the coexpression of GFP. The expression of GFP was used to confirm transgene expression, specifically in the LC and not adjacent structures. At 1-3 mo p.i., a one-way ANOVA with a between-subjects factor of Group (htauE14, AAV-GFP, and control) revealed a significant effect of Group, $F(2, 12) = 257.29$, $p < 0.001$. Tukey's HSD test indicated that the mean score for htauE14 animals ($M = 93.72$ %, $SD = 5.70$%) was significantly higher than AAV-GFP ($M = 48.56$%, $SD = 10.55$%), and control animals ($M = 0.08$%, $SD = 0.16$%). Furthermore, AAV-GFP animals had a significantly higher percentage of coexpression compared to vehicle-control animals (see Figure 2A).

At 4-6 mo p.i., an independent samples *t*-test revealed that htauE14 rats ($M = 96.35$%, $SD = 1.10$%) had a significantly higher coexpression percentage compared to control rats ($M = 0.21$%, $SD = 0.30$%), $t(3) = 115.35$, $p < 0.001$, Cohen's $d = 105.30$ (see Figure 2B).

3.2. Hippocampus DβH Densitometry

To chronicle the changes in the LC-temporal lobe projections, immunohistochemistry was performed using an antibody against the synthesizing enzyme

for norepinephrine, DβH, in htauE14 and control animals. Sections were divided into dorsal and ventral hippocampus, with any section below -5.6 mm being classified as ventral and anything at or above -5.6 mm being classified as dorsal. Furthermore, animals were put into one of two categories based on survival times post-LC-infusion. Animals were grouped into either the 1-3- or 4-6 months p.i. group. Independent samples *t*-tests were conducted on the mean of the adjusted relative optical densities for each group for each region of the hippocampus. The adjusted relative optical density for each section was calculated by subtracting the corresponding ROD measurement from a no antibody control from each corresponding measurement.

1-3 months post-infusion. Independent samples *t*-tests on the adjusted dorsal hippocampus ROD measurements revealed that at 1-3 months post-infusion, htauE14 animals had higher ROD values than control animals for CA1 oriens, $t(1) = 35.29$, $p = 0.02$, CA3 lucidum, $t(1) = 111.36$, $p = 0.006$, hilus, $t(1) = 14.70$, $p = 0.04$, and the outer molecular layer, $t(1) = 24.96$, $p = 0.03$.

Independent samples *t*-tests on the adjusted ventral hippocampus ROD measurements revealed that at 1-3 months post-infusion, htauE14 animals had higher ROD values than control animals for CA1 lacunosum moleculare, $t(1) = 3.54$, $p = 0.01$, CA1 oriens, $t(1) = 6.51$, $p < 0.001$, CA1 pyramidal, $t(1) = 6.24$, $p < 0.001$, CA1 radiatum, $t(1) = 5.13$, $p < 0.001$, medial molecular layer, $t(1) = 2.63$, $p = 0.03$, and subgranular zone, $t(1) = 2.31$, $p = 0.05$ (see Figure 3C-E).

4-6 months post-infusion. Independent samples *t*-tests on the adjusted dorsal and ventral hippocampus ROD measurements revealed that at 4-6 months post-infusion,

htauE14 animals did not have significantly different adjusted ROD values than controls (see Figure 4C-E).

3.3. Entorhinal Cortex, Presubiculum, and Parasubiculum DβH Densitometry

1-3 months post-infusion. Independent samples *t*-tests on the adjusted dorsal EC and dorsal subiculum ROD measurements revealed that at 1-3 months post-infusion, htauE14 animals had higher ROD values than control animals for LEC-I, $t(1) = 32.28$, $p = 0.02$, LEC-II, $t(1) = 14.98$, $p = 0.04$, MEC-I, $t(1) = 30.41$, $p = 0.02$, MEC-V/VI, $t(1) = 291.61$, $p = 0.002$, parasubiculum, $t(1) = 75.12$, $p = 0.008$, and presubiculum, $t(1) = 45.49$, $p = 0.014$.

Independent samples *t*-tests on the adjusted ventral EC and ventral subiculum ROD measurements revealed that at 1-3 months post-infusion, htauE14 animals had higher ROD values than control animals for MEC-I, $t(1) = 2.34$, $p = 0.047$ (see Figure 5A-C).

4-6 months post-infusion. Independent samples *t*-tests on the adjusted dorsal and ventral EC and subiculum ROD measurements revealed that at 4-6 months post-infusion, htauE14 animals did not have significantly different adjusted ROD values than controls (see Figure 5D-F).

3.4. Evaluation of Behavioural Test Battery

3.4.1. Spontaneous Alternation

We assessed spatial working memory using the spontaneous alternation task described by Galeano et al. (2014). The percentage of alternation data from the Spontaneous Alternation task were analyzed using a two-way between-subjects ANOVA,

with the between-subjects factors being Sex (male, female) and Group (htauE14, control). As described by Galeano et al. (2014), the percentage of alternation was calculated by dividing the actual number of alternations by the maximum number of alternations and multiplying by 100. The maximum number of alternations was calculated by subtracting two from the total number of arm entries. An animal with a low percentage of alternation was considered impaired in terms of spatial working memory due to an inability to remember which arm was previously visited. While data from the first 3, 5, and 8 minutes were analyzed, only data from the first three minutes are presented for a more sensitive analysis and to control for the effects of habituation and fatigue.

At 1-3 mo. p.i., the main effect of Sex, $F(1, 44) = 14.68$, $p < 0.001$, $\eta_p^2 = 0.25$, and the Sex × Group interaction, $F(1, 44) = 6.48$, $p = 0.014$, $\eta_p^2 = 0.13$, were found to be statistically significant. The main effect of Group was not found to be statistically significant (see Figure 6A).

Post hoc comparisons using Tukey's HSD test on the Sex × Group interaction found that control females ($M = 70.01\%$, $SD = 14.67\%$) had a significantly higher percentage of alternation than control males ($M = 34.13\%$, $SD = 18.93\%$) and htauE14 males ($M = 43.73\%$, $SD = 22.96\%$).

At 4-6 mo. p.i., both main effects and the interaction were not statistically significant when analyzing the percentage of alternation for the first 3 minutes of the task (see Figure 6B).

3.4.2. Novel Object Recognition

Hippocampal-independent recognition memory was assessed using a two-trial novel object recognition test. For the novel object recognition task, the data of interest was the percentage of time spent in each arm of the Y-maze during the test phase. The percentage was calculated by dividing the amount of time spent in one of the three arms by the total amount of time spent in all three arms and was multiplied by 100. These data were analyzed using a three-way mixed-design ANOVA, with a within-subjects factor of Arm (Start, Familiar, Novel), and two between-subjects factors of Sex (male, female) and Group (htauE14, control). At 1-3 months, the main effect of Arm, $F(2, 88) = 4.99$, $p = 0.009$, $\eta_p^2 = 0.10$, was found to be statistically significant. All other main effects and interactions were not found to be statistically significant (see Figure 7A).

Post hoc comparisons using Tukey's HSD test on the main effect of Arm revealed that animals spent a significantly greater percentage of time in the Novel arm (M = 39.29%, SD = 12.40%) than the Familiar Arm (M = 28.59%, SD = 12.91%).

At 4-6 months, the data were analyzed using a three-way mixed-design ANOVA as described above for 1-3 months. Similar to animals tested at 1-3 months, the main effect of Arm, $F(2, 88) = 11.85$, $p < 0.001$, $\eta_p^2 = 0.21$, was found to be statistically significant. All other main effects and interactions were not found to be statistically significant (see Figure 7B).

Post hoc comparisons using Tukey's HSD test on the main effect of Arm revealed that animals, again, spent a significantly greater percentage of time in the Novel arm (M = 41.29%, SD = 12.58%) than the Familiar Arm (M = 32.80%, SD = 12.96%), and the Start arm (M = 25.91%, SD = 12.19%).

3.4.3. Morris Water Maze

The Morris water maze task was used to assess spatial long-term memory in our animals and consisted of three phases.

Cued learning. The cued phase of the task was used to rule out perceptual, motivational and motoric differences between groups. The latency data were analyzed using a three-way mixed-design ANOVA, one for each sex, with two within-subjects factors of Trial and Day (4 trials/day) and a between-subjects factor of Group (htauE14, control).

For females at 1-3 mo. p.i., the main effect of Trial, $F(3, 78) = 18.26$, $p < 0.001$, $\eta_p^2 = 0.41$, and the main effect of Day, $F(1, 26) = 78.23$, $p < 0.001$, $\eta_p^2 = 0.75$, were found to be statistically significant, with animals taking less time to find the platform across trials and days. There was also a significant Trial × Day interaction $F(3, 78) = 5.78$, $p = 0.001$, $\eta_p^2 = 0.18$, reflecting acquisition of the task (see Figure 8A). All other main effects and interactions were not found to be significant.

For males at 1-3 mo. p.i., the main effect of Trial, $F(3, 63) = 5.76$, $p = 0.002$, $\eta_p^2 = 0.22$, and the main effect of Day, $F(1, 21) = 30.76$, $p < 0.001$, $\eta_p^2 = 0.59$, were found to be statistically significant, with animals taking less time to find the platform across trials and days. The Trial × Day interaction $F(3, 63) = 15.50$, $p < 0.001$, $\eta_p^2 = 0.42$, was also found to be significant, reflecting acquisition of the task (see Figure 8D). All other main effects and interactions were not found to be significant.

For females at 4-6 mo. p.i., the main effect of Trial, $F(3, 54) = 7.93$, $p < 0.001$, $\eta_p^2 = 0.31$, and the main effect of Day, $F(1, 18) = 31.04$, $p < 0.001$, $\eta_p^2 = 0.63$, were found to

be statistically significant, with animals taking less time to find the platform across trials and days. All other main effects and interactions were not found to be significant (see Figure 9A).

For males at 4-6 mo. p.i., the main effect of Trial, $F(3, 54) = 11.62$, $p < 0.001$, $\eta_p^2 = 0.39$, and the main effect of Day, $F(1, 18) = 25.11$, $p < 0.001$, $\eta_p^2 = 0.58$, were found to be statistically significant, with animals taking less time to find the platform across trials and days. The Trial × Day interaction $F(3, 54) = 3.96$, $p = 0.013$, $\eta_p^2 = 0.18$, was also found to be significant, reflecting acquisition of the task (see Figure 9D). All other main effects and interactions were not found to be significant.

Hidden learning. The hidden phase of the task was used to test hippocampal-dependent spatial memory. At 1-3 months, the latency data were analyzed using a four-way mixed-design ANOVA, with two within-subjects factors of Trial and Day (4 trials/day) and two between-subjects factors of Sex (male, female) and Group (htauE14, control). Mauchly's test of sphericity was violated for the main effect of Day, Mauchly's $W = 0.34$, $p < 0.001$; therefore, degrees of freedom were corrected using Greenhouse-Geisser estimates of sphericity, $\varepsilon = 0.72$. The main effects of Trial, $F(3, 138) = 14.22$, $p < 0.001$, $\eta_p^2 = 0.24$, and Day, $F(2.87, 132.14) = 74.94$, $p < 0.001$, $\eta_p^2 = 0.62$, were found to be statistically significant, with animals taking less time to find the platform across trials and days. The main effect of Sex, $F(1, 46) = 6.95$, $p = 0.01$, $\eta_p^2 = 0.13$, was found to be statistically significant with females ($M = 19.61$s, $SD = 6.69$s) taking longer to find the platform than males ($M = 15.50$s, $SD = 5.16$s). The main effect of Group and all interactions were not found to be statistically significant (see Figure 8B/E).

As can be seen in Figure 8E, there appeared to be a difference between groups for males on Day 1; as a result, independent samples *t*-tests for each Sex for each Day were conducted. An independent samples *t*-test revealed that htauE14 males (M = 38.35s, SD = 14.03s) took significantly longer to locate the platform than control males (M = 25.17s, SD = 7.87s) on Day 1, $t(20) = 2.78$, $p = 0.01$, Cohen's $d = 1.19$. Groups did not significantly differ on any other day. Furthermore, female htauE14 rats did not differ significantly from controls on each of the five days (see inset graph of Figure 8E).

At 4-6 months, the data were analyzed using a four-way mixed-design ANOVA, as previously described. Mauchly's test of sphericity was violated for the main effect of Trial, Mauchly's W = 0.71, $p < 0.04$, Day, Mauchly's W = 0.31, $p < 0.001$, and the Trial × Day interaction, Mauchly's W = 0.00, $p < 0.001$; therefore, degrees of freedom were corrected using Greenhouse-Geisser estimates of sphericity for the main effect of Day, $\varepsilon = 0.61$ and the Trial × Day interaction, $\varepsilon = 0.48$. For the main effect of Trial, the degrees of freedom were corrected using the Huynh-Feldt estimate of sphericity, $\varepsilon = 0.92$. The main effects of Trial $F(2.76, 96.51) = 5.21$, $p = 0.003$, $\eta_p^2 = 0.13$, and Day, $F(2.42, 84.78) = 31.80$, $p < 0.001$, $\eta_p^2 = 0.48$, were found to be statistically significant, with animals taking less time to find the platform across trials and days. The main effect of Sex, $F(1, 35) = 5.57$, $p = 0.02$, $\eta_p^2 = 0.14$, was found to be statistically significant, with females (M = 12.44s, SD = 3.51s) taking longer to find the platform than males (M = 9.79s, SD = 3.45s). The Trial × Day interaction was found to be statistically significant, $F(5.77, 201.83) = 6.34$, $p < 0.001$, $\eta_p^2 = 0.15$, reflecting acquisition of the task. The main

effect of Group and all other interactions were not found to be statistically significant (see Figure 9B/E).

To see if there was a difference between groups each day, independent samples *t*-tests for each Sex for each Day were conducted. Independent samples *t*-tests revealed that htauE14 males did not differ significantly from control males in their mean latency to find the platform on each of the five days. Furthermore, female htauE14 rats did not differ significantly from control females on each of the five days.

Probe trial. The Probe trial was used to assess retention or memory of the platform location. During this trial, the hidden platform was removed, and the time spent swimming in the target quadrant was recorded. At 1-3 months, the time spent in the target quadrant on the probe trial was analyzed using a two-way ANOVA with two between-subjects factors of Sex (male, female) and Group (htauE14, control). The main effect of Sex, $F(1, 46) = 5.13$, $p = 0.03$, $\eta_p^2 = 0.10$, was found to be statistically significant with males ($M = 29.00$s, $SD = 7.52$s) spending more time in the target quadrant than females ($M = 24.25$s, $SD = 7.03$s) (see Figure 8C/F).

At 4-6 months, the probe data were analyzed using a two-way ANOVA, as described above. The main effects of Group, $F(1, 35) = 0.03$, $p = 0.87$, $\eta_p^2 = 0.00$, and Sex, $F(1, 35) = 1.95$, $p = 0.17$, $\eta_p^2 = 0.05$ were not found to be statistically significant. Furthermore, the Group × Sex interaction, $F(1, 35) = 0.07$, $p = 0.79$, $\eta_p^2 = 0.00$ was not statistically significant (see Figure 9C/F).

3.4.4. Radial Arm Maze

The data of interest for the RAM training were the trials to criterion (8 out of 10 consecutive trials correct) for the more difficult, adjacent arm version of the task. These data were analyzed using a two-way ANOVA, with between-subjects factors of Sex (male, female) and Group (htauE14, control). At 1-3 and 4-6 months p.i., the Sex and Group main effects and the Sex × Group interaction were not found to be significant (see Figure 10).

4. Discussion

Using an adeno-associated virus, we selectively inserted a gene for pseudophosphorylated human tau into the LC of heterozygous TH:Cre male and female rats to create a rat model of pretangle AD. Using our animal model of preclinical AD, we monitored the behavioural and anatomical consequences of LC-htauE14 in rats at 1-3 and 4-6 months p.i.

4.1. AAV-htauE14-GFP is Highly Expressed in LC Neurons

Using an antibody for the NE synthesizing enzyme TH to identify LC neurons, we confirmed GFP colocalization in LC neurons; we used GFP as an indicator of transgene expression. At 1-3 mo p.i., htauE14 and AAV-GFP animals differed significantly, with htauE14 animals showing higher transduction rates; this may be due to small sample sizes, although this is unlikely. It is also unlikely that this difference is due to using a FLEX genetic switch in the AAV-GFP infused animals and a DIO in htauE14 animals. Both switches are Cre-On, act via the Cre-LoxP system, and use two wild-type and two mutant LoxP sites (Xu & Zhu, 2018). Immunohistochemistry showed that in htauE14 animals at 1-3 months, the majority of TH^+ LC cells (93.7%) were also GFP^+. Expression

in AAV-GFP animals was much lower, with 48.6% colocalization of TH^+GFP^+. In LC-htauE14 infused animals at 4-6 months post-infusion, 96.4% of TH^+ LC neurons were also GFP^+. The level of LC selective expression observed in our htauE14 infused animals is consistent with previous studies that observed colocalization in 90-93% of LC neurons (Gompf et al., 2015; Lerchner et al., 2014). Using non-human primates, Lerchner et al. infused a lentivirus carrying GFP bilaterally in the LC of their subjects. Coexpression of TH and GFP revealed that 90% of TH^+ LC neurons expressed GFP. Furthermore, Ghosh et al. (2019) showed that, on average, 83% of $D\beta H^+$ LC neurons were GFP^+; this finding parallels our finding of high transfection rates of AAV-htauE14 in the LC of TH:Cre rats.

In a chemogenetic study, Vazey and Aston-Jones (2014) infused an AAV containing the DREADD receptor, hMD3Dq, or mCherry directed at the LC. They observed high penetrance with 97% $TH^+hMD3Dq^+$ and $TH^+/mCherry^+$ colocalized cells. While we used a different transgene and promotor, like Vazey and Aston-Jones (2014), we observed similar selective expression levels in the LC of our htauE14 animals. Additionally, in their chemogenetic study, Stevens et al. (2020) infused an AAV2/7 vector with the DREADD receptor, hMD3Dq, with mCherry, and observed that, on average, 20.6% of LC neurons were $hMD3Dq^+$. This is much lower than our penetrance rates for our control GFP virus and may be due to a difference in the serotype and the binding affinity of their vector to the cell surface receptors on LC neurons as serotype has been shown to be important for specificity and expression rates. While serotype may have influenced specificity and expression rates, their use of the PRSx8 promotor may have influenced their results.

Our research supports AAV2/9 vectors as being a suitable method for transgene delivery with our high rates of penetrance and specificity. Future directions in colocalization research should attempt to delineate any differences or confounds that resulted in penetrance differences between the two groups. Differences in cell density and numbers could be included in future studies to better understand the observed difference between AAV-GFP and htauE14 animals.

4.2. DβH$^+$ Fibre Density is Higher in CA1 and the Subgranular Zone in htauE14 Rats

Densitometry was conducted on brightfield images of DβH immunoreactivity in the hippocampus and entorhinal cortex. Three major regions of the hippocampus, DG CA1 and CA3, were further divided into subregions. Analysis of the average RODs of these regions revealed that htauE14 animals had a significantly higher ROD in all four subregions of ventral CA1. While this effect was not seen in dorsal CA1, visual inspection would suggest a trend similar to that of ventral CA1. With more subjects, this trend may be significant.

As CA1 of the hippocampus has been shown to be important in spatial learning and memory (Tsien et al., 1996), our increase in DβH$^+$ fibre density in CA1 may explain why htauE14 animals were not impaired on the RAM and MWM tasks. This sprouting of DβH$^+$ fibres may act as a compensatory mechanism and help maintain hippocampal circuitry. Furthermore, this increase in fibre density is consistent with previous studies that observe fibre sprouting as a result of brain damage (Harkany et al., 2000; Phinney et al., 1999). A more detailed morphological analysis of fibre thickness and varicosity

numbers should be included in future studies. Additionally, the effects of pathological effects of htauE14 on axonal sprouting in not only CA1, but other brain regions should be monitored at later timepoints to see if fibre retraction correlates with memory impairments.

Interestingly, this magnitude of an effect was not observed in CA3 or the DG. CA1 is the primary output of the hippocampus and is the first region of the hippocampus affected in the early stages of Alzheimer disease (Neuman et al., 2015; Small et al., 2011). Furthermore, AD pathology is thought to progress in a ventral to dorsal direction (Neuman et al., 2015). While more subjects are needed, at 4-6 months, there appears to be a trend for higher ROD measurements in htauE14 animals in dorsal CA1.

Furthermore, htauE14 animals also displayed higher ROD levels in the SGZ of the hippocampus. In the brains of adult humans and rodents, neurogenesis has been shown to take place in the SGZ (Ehninger & Kempermann, 2007; Kempermann et al., 1997; Kuhn et al., 1996). Wnt/β-catenin is a signalling factor critical for regulating neurogenesis in the hippocampus (Abril et al., 2013; Sato et al., 2003). When wnt signalling is overexpressed in the SGZ, neurogenesis occurs. In the Alzheimer brain, wnt signalling is deregulated, and, as a result, neurogenesis is decelerated and may even cease to occur (Folke et al., 2018; Okamoto et al., 2011). Future investigation of the wnt signalling pathway, and markers of neurogenesis could explain the impact of abnormally phosphorylated tau in the LC on neurogenesis in our animal model of AD.

In contrast to our findings, others have observed reductions in $D\beta H^{+}$ fibres in their AD models (Ghosh et al., 2019; Rorabaugh et al., 2017). Using TgF344-AD rats

heterozygous for an APP_{sw}/PS1ΔE9, Rorabaugh et al. (2017) observed the effects of mutant amyloid precursor protein and presenilin-1 on fibre density in mEC and hippocampus. Immunohistochemistry using DβH revealed a significant genotype × age interactions, with 16-month-old TgF344-AD rats having significantly reduced $D\beta H^+$ fibre density in the dentate gyrus compared to 16-month-old TgF344-AD and control animals. This age-dependent reduction in $D\beta H^+$ fibre density was also observed in CA1 and CA3 of the hippocampus. In agreement with these findings, Ghosh et al. (2019) observed a reduction in $D\beta H^+$ fibre density in the piriform cortex of 11-month-old htauE14 rats compared to non-infused and GFP controls 7-8 months post-infusion. Our increase in fibre density suggests further exploration is needed. In comparison to these studies, our animals were subjected to a more extensive battery. The influence of such substantial enrichment may ameliorate potential cognitive impairment and should be studied. Furthermore, we sampled animals at earlier timepoints and conducted a more extensive analysis of hippocampal brain regions, which may explain this difference. Sampling at earlier time points and from many brain regions provides a clearer picture of how LC-htauE14 affects behaviour and brain morphology from a young age.

4.3. Behavioural Effects of LC-htauE14

4.3.1. Control Females Alternate More at 1-3 Months Post-Infusion

In spontaneous alternation testing for spatial working memory, female rats in the control group had a significantly higher percentage of alternation than htauE14 and control males at 1-3 months p.i. This finding may be due to sex-dependent differences in structures used for spatial working memory. Méndez-López et al. (2009) used the Morris

water maze to assess male and female Wistar rats' spatial working memory. In their version of the task, animals received two consecutive trials, a sample and retention trial used to assess short-term memory. During the sample trial, animals were released from one of four start points and trained to locate a platform. During the retention trial, the platform was removed, and animals were expected to recall the location of the platform from the sample trial. The platform location was different each day so that the same platform location was not used the previous three days. While no behavioural differences were found, they observed differences in the activity of various brain regions. Males tended to use hippocampal-centred navigation, while females used areas related to the prefrontal cortex to aid them in spatial navigation. Furthermore, this study tested females during different phases of the estrous cycle to counterbalance hormonal status as a potential confounding variable. Their findings suggest that acquisition of their version of the MWM is mediated by different brain regions in a sex-dependent manner.

Interestingly, female controls did not differ from any other groups at 4-6 months p.i. As the second test was conducted in the same apparatus and room, this may be due to habituation to a now-familiar environment. Future studies should test animals in a novel environment with each iteration of the task to determine whether this lack of an effect is due to familiarity of the environment or to some other factor, such as ageing.

Using a two-trial version of the spontaneous alternation task, which involved an animal being removed after making an arm choice, researchers found that animals with lesions to several subdivisions of the prefrontal cortex displayed impairments in spontaneous alternation (Divac et al., 1975; Mogensen & Divac, 1993). While lesions to the prefrontal cortex impair spontaneous alternation, other brain regions such as the

hippocampus (Means et al., 1971; Stevens & Cowey, 1973), medial raphe (Asin & Fibiger, 1984) and entorhinal cortex (Ramirez & Stein, 1984) have also been implicated. Examining brain regions important in completing our version of the task could help better explain this finding. Furthermore, performance on spontaneous alternation tests can be confounded by attention and motivation; it is recommended that this test not be the sole test of spatial working memory, especially our free-running version (Hughes, 2004).

4.3.2. LC-htauE14 Does Not Impair Hippocampal-Independent Memory in the Novel Object Recognition Task of Long-Term Memory

Both htauE14 and control animals performed similarly on the novel object recognition task. While there was no effect of Group or Sex, there was an effect of Arm, with animals spending significantly more time in the Novel arm than the Start and Familiar arm. This effect was seen at both 1-3 and 4-6 months p.i. These findings suggest that LC-htauE14 did not produce impairments in this hippocampal-independent test of long-term memory.

The perirhinal cortex has consistently been shown to be implicated in object recognition memory (Ennaceur et al., 1996; Mumby & Pinel, 1994; Winters & Bussey, 2005). Ennaceur et al. (1996) showed that neurotoxic lesions to the fornix and perirhinal cortex produced opposite effects in spatial versus nonspatial memory tasks. Animals with lesions to the fornix displayed behavioural deficits on spatial memory tests, such as a T-maze alternation task and a spatial lever discrimination task; however, animals were not impaired on a test that assessed object recognition. For animals with perirhinal lesions, the opposite was true; that is, animals spent a similar amount of time exploring the novel

and familiar objects. These findings point to a dissociation between the hippocampus and the perirhinal cortex and that lesions to either of these systems produce distinct effects.

Additionally, Winters and Bussey (2005) showed that transient inactivation of the perirhinal cortex using lidocaine impaired object recognition using the spontaneous object recognition task. This task consisted of a sample and a choice phase. During the sample phase, animals were placed in a Y-maze and allowed to explore two arms that contained identical objects. Animals were then removed for the retention delay, which lasted from 5 minutes to 180 minutes. During the choice phase, animals were placed back in the Y-maze with one identical object and one novel object. To quantify object recognition, they used a discrimination ratio, which was the difference in time exploring the novel and familiar objects divided by the total time exploring both objects. Winters and Bussey (2005) found that animals that received lidocaine infusions prior to the sample phase were significantly impaired compared to controls; that is, they had lower discrimination ratios, regardless the length of the retention delay. Furthermore, rats that received lidocaine infusions immediately or 20 minutes after the sample phase were impaired on the choice phase. These findings further support the role of the perirhinal cortex for the encoding, consolidation, and retrieval of object recognition memory.

To better understand the effects of LC-htauE14 on object recognition memory, longitudinal monitoring of behaviour on the novel object test should be monitored in conjunction with anatomical changes in the perirhinal cortex. Outlining the anatomical spread of LC-htauE14 could better explain our findings.

4.3.3. htauE14 Males are Impaired Early on in Morris Water Maze Training at 1-3 Months Post-Infusion

The cued phase of the MWM was used to ensure that there were no perceptual, motivational and motoric differences between groups that could influence performance during the Hidden and Probe phases. No group differences were observed, so we could proceed with our analysis and rule out the mentioned confounds.

From the Hidden phase of the MWM task, we found no evidence that htauE14 produced deficits in spatial memory when locating a hidden platform. Overall, at 1-3 and 4-6 months, htauE14 animals performed similarly to controls. Interestingly, on the first day of the Hidden phase at 1-3 months, htauE14 males took significantly longer to locate the platform than control males. This impairment was not observed for the rest of the Hidden phase or when animals were tested again at 4-6 months. In line with this finding, Rorabaugh et al. (2017) observed that TgF344-AD rats had higher latencies to find the platform than controls at the beginning of their acquisition training but then acquired the task similar to controls.

While htauE14 males displayed impairments early on, these animals quickly acquired the task and demonstrated normal spatial learning and memory. Since spatial processing relies on an interaction between various brain regions, this improvement in spatial memory can be attributed to compensation by other components of the network (Xu et al., 2014). Therefore, while compromising some regions important to spatial learning can produce impairments in behaviour, this impairment will be transient unless multiple regions of the network are compromised so that compensation by other regions is less likely. Additionally, it is also possible that initial acquisition is impaired; however,

once the task is learned, animals are able to recall the task requirements and successfully complete the task.

The Probe trial was used to detect differences in retention of the task or perseveration in searching strategies in the LC-htauE14 infused and control groups. At 1-3 months, the main effect of Sex was observed, with males spending more time in the target quadrant than females. This impairment in females during the Probe trial has been reported elsewhere (Clinton et al., 2007).

Using a mouse model of AD that possessed three dementia-relevant transgenes, $PS1_{M146v}$, tau_{P301L} and APP_{SWE}, Clinton et al. (2007) showed that at 6- and 9-months of age, females displayed more significant cognitive deficits during both acquisition and probe phases of the MWM, in comparison to age-matched males. However, this difference diminished when animals were assessed at 12-months of age. To explore this difference, corticosterone levels were measured 30 minutes post-water maze training. It was found that young (9-month old) female mice had significantly higher corticosterone levels than their age-matched male counterparts. This difference in corticosterone levels was not observed in older mice. This finding suggests that higher corticosterone levels may lead to poorer performance on the MWM task.

In our study, females appear to be different in comparison to males during the probe trial at 1-3 months as they spent less time in the correct quadrant. This difference was not observed at 4-6 months. This finding is similar to that of Clinton et al. (2007) and suggests that elevated serum corticosterone levels may explain our findings. It is possible that animals may experience a higher stress response initially; however, once habituated, these effects may no longer be observed. Future studies should examine differences in the

stress-response exhibited on aversive behavioural tasks to probe for group and sex differences that could explain cognitive deficits.

4.3.4. LC-htauE14 Does Not Impair Performance on the Radial Arm Maze Task

The radial arm maze is an apparatus commonly used to assess spatial working and reference memory. To assess place learning, we used a version of the RAM modelled after McDonald and White (1995) that required animals to discriminate between a food-arm and one of two no-food arms. McDonald and White (1995) found that animals with fornix-fimbria lesions were impaired on this version of the task compared to controls and animals with lesions to the striatum and amygdala. These findings suggest that active place learning requires an active hippocampal system, while the striatum and amygdala are not crucial for the acquisition of this version of the task. With our eight-arm maze, animals were trained to discriminate between a food and a no-food arm that were 45° apart. Future studies should assess if using a maze more arms (e.g., 12- or 16-arm maze), resulting in a reduction in the degree separation in arms, would produce a more challenging version due to greater overlap in the cues available at both arms. A more difficult task may be more sensitive to detect differences between groups.

5. Conclusion

This research revealed that LC-htauE14 transiently impaired performance in htauE14 males on the first day of the Hidden phase of the MWM when tested 1-3 months p.i. This impairment early in training, but compensation later has been reported previously. Future directions should examine neural recruitment as a potential explanation for this compensation. Furthermore, differences in results from our

densitometry analysis using DβH suggest an influence of abnormal tau on the hippocampus. DβH analysis of the hippocampus revealed that CA1 of the hippocampus might be affected by LC-htauE14; this is consistent with what is observed in AD patients. While LC-htauE14 appears to initiate changes in the brains, the observable effects of this protein on behaviour are limited. It is possible that it is too early for the spread of abnormal tau to produce any observable behavioural deficits. Furthermore, our study used an extensive test battery providing animals with more enrichment compared to other studies. This enrichment may account for our finding of increased fibre density. Future directions may include comparing enriched to non-enriched animals. To our knowledge, we are the first to report high penetrance of AAV2/9- htauE14 and the consequent effects of LC-htauE14 on behaviour and anatomy. Future research should monitor the behavioural and anatomical changes that occur past seven months after infusion of tau in the locus coeruleus.

References

Alonso, A. D., Cohen, L. S., Corbo, C., Morozova, V., ElIdrissi, A., Phillips, G., & Kleiman, F. E. (2018). Hyperphosphorylation of tau associates with changes in its function beyond microtubule stability. *Frontiers in Cellular Neuroscience, 12*, 1-12. https://doi.org/10.3389/fncel.2018.00338

Amaral, D., & Sinnamon, H. (1977). The locus coeruleus: neurobiology of a central noradrenergic nucleus. *Progress in Neurobiology, 9*(3), 147-196. https://doi.org/10.1016/0301-0082(77)90016-8

Andrés-Benito, P., Fernández-Dueñas, V., Carmona, M., Escobar, L. A., Torrejón-Escribano, B., Aso, E., Ciruela, F., & Ferrer, I. (2017). Locus coeruleus at asymptomatic early and middle Braak stages of neurofibrillary tangle pathology. *Neuropathology and Applied Neurobiology, 43*(5), 373-392. https://doi.org/10.1111/nan.12386

Asin, K. E., & Fibiger, H. C. (1984). Spontaneous and delayed spatial alternation following damage to specific neuronal elements within the nucleus medianus raphe. *Behavioural Brain Research, 13*(3), 241-250. https://doi.org/10.1016/0166-4328(84)90166-9

Aston-Jones, G., Rajkowski, J., & Cohen, J. (1999). Role of locus coeruleus in attention and behavioral flexibility. *Biological Psychiatry, 46*(9), 1309-1320. https://doi.org/10.1016/S0006-3223(99)00140-7

Bancher, C., Brunner, C., Lassmann, H., Budka, H., Jellinger, K., Wiche, G., Seitelberger, F., Grundke-Iqbal, I., Iqbal, K., & Wisniewski, H. M. (1989). Accumulation of abnormally phosphorylated tau precedes the formation of neurofibrillary tangles in Alzheimer's disease. *Brain Research, 477*(1-2), 90-99. https://doi.org/10.1016/0006-8993(89)91396-6

Benarroch, E. E. (2009). The locus ceruleus norepinephrine system: Functional organization and potential clinical significance. *Neurology, 73*(20), 1699-1704. https://doi.org/10.1212/WNL.0b013e3181c2937c

Bertram, L., & Tanzi, R. E. (2005). The genetic epidemiology of neurodegenerative disease. *Journal of Clinical Investigation, 115*(6), 1449-1457. https://doi.org/10.1172/JCI24761

Betts, M. J., Kirilina, E., Otaduy, M. C. G., Ivanov, D., Acosta-Cabronero, J., Callaghan, M. F., Lambert, C., Cardenas-Blanco, A., Pine, K., Passamonti, L., Loane, C., Keuken, M. C., Trujillo, P., Lüsebrink, F., Mattern, H., Liu, K. Y., Priovoulos, N., Fliessbach, K., Dahl, M. J., Maaß, A., Madelung, C. F., Meder, D., Ehrenberg, A. J., Speck, O., Weiskopf, N., Dolan, R., Inglis, B., Tosun, D., Morawski, M., Zucca, F. A., Siebner, H. R., Mather, M., Uludag, K., Heinsen, H., Poser, B. A., Howard, R., Zecca, L., Rowe, J. B., Grinberg, L. T., Jacobs, H. I. L., Düzel, E., & Hämmerer, D. (2019). Locus coeruleus imaging as a biomarker for noradrenergic dysfunction in neurodegenerative diseases. *Brain, 142*(9), 2558-2571. https://doi.org/10.1093/brain/awz193

Bharani, K. L., Derex, R., Granholm, A.-C., & Ledreux, A. (2017). A noradrenergic lesion aggravates the effects of systemic inflammation on the hippocampus of aged rats. *PLoS One, 12*(12), 1-20. https://doi.org/10.1371/journal.pone.0189821

Blackstad, T. W., & Flood, P. R. (1963). Hippocampus of the brain: Ultrastructure of hippocampal axo-somatic synapses. *Nature, 198*(4880), 542-543. https://doi.org/10.1038/198542a0

Braak, H., Alafuzoff, I., Arzberger, T., Kretzschmar, H., & Del Tredici, K. (2006). Staging of Alzheimer disease-associated neurofibrillary pathology using paraffin sections and immunocytochemistry. *Acta Neuropathologica, 112*(4), 389-404. https://doi.org/10.1007/s00401-006-0127-z

Braak, H., & Braak, E. (1991). Neuropathological stageing of Alzheimer-related changes. *Acta Neuropathologica, 82*(4), 239-259. https://doi.org/10.1007/BF00308809

Braak, H., & Del Tredici, K. (2011). The pathological process underlying Alzheimer's disease in individuals under thirty. *Acta Neuropathologica, 121*(2), 171-181. https://doi.org/10.1007/s00401-010-0789-4

Braak, H., & Del Tredici, K. (2012). Where, when, and in what form does sporadic Alzheimer's disease begin? *Current Opinion in Neurology, 25*(6), 708-714. https://doi.org/10.1097/WCO.0b013e32835a3432

Braak, R. H., Thal, R. D., Ghebremedhin, R. E., & Del Tredici, R. K. (2011). Stages of the pathologic process in Alzheimer Disease: Age categories from 1 to 100 years. *Journal of Neuropathology and Experimental Neurology, 70*(11), 960-969. https://doi.org/10.1097/NEN.0b013e318232a379

Brunden, K. R., Ballatore, C., Crowe, A., Smith, A. B., Lee, V. M. Y., & Trojanowski, J. Q. (2010). Tau-directed drug discovery for Alzheimer's disease and related tauopathies: A focus on tau assembly inhibitors. *Experimental Neurology, 223*(2), 304-310. https://doi.org/10.1016/j.expneurol.2009.08.031

Busser, J., Geldmacher, D. S., & Herrup, K. (1998). Ectopic cell cycle proteins predict the sites of neuronal cell death in Alzheimer's disease brain. *The Journal of Neuroscience, 18*(8), 2801-2807. https://doi.org/10.1523/jneurosci.18-08-02801.1998

Canto, C., B, Floris, G. W., & Menno, P. W. (2008). What does the anatomical organization of the entorhinal cortex tell us? *Journal of Neural Transplantation & Plasticity, 2008*, 1-18. https://doi.org/10.1155/2008/381243

Chalermpalanupap, T., Schroeder, J. P., Rorabaugh, J. M., Liles, L. C., Lah, J. J., Levey, A. I., & Weinshenker, D. (2018). Locus coeruleus ablation exacerbates cognitive deficits, neuropathology, and lethality in P301S tau transgenic mice. *The Journal of neuroscience, 38*(1), 74-92. https://doi.org/10.1523/JNEUROSCI.1483-17.2017

Chow, V., Mattson, M., Wong, P., & Gleichmann, M. (2010). An Overview of APP Processing Enzymes and Products. *NeuroMolecular Medicine, 12*(1), 1-12. https://doi.org/10.1007/s12017-009-8104-z

Clinton, L. K., Billings, L. M., Green, K. N., Caccamo, A., Ngo, J., Oddo, S., McGaugh, J. L., & LaFerla, F. M. (2007). Age-dependent sexual dimorphism in cognition and stress response in the 3xTg-AD mice. *Neurobiology of Disease, 28*(1), 76-82. https://doi.org/10.1016/j.nbd.2007.06.013

Cummings, J., & Fox, N. (2017). Defining disease modifying therapy for Alzheimer's disease. *The Journal of Prevenetaion of Alzheimer's Disease, 4*(2), 109-115. https://doi.org/10.14283/jpad.2017.12

Cummings, J. L., Morstorf, T., & Zhong, K. (2014). Alzheimer's disease drug-development pipeline: few candidates, frequent failures. *Alzheimer's Research & Therapy, 6*(4), 37-37. https://doi.org/10.1186/alzrt269

Dahl, D., & Sarvey, J. M. (1989). Norepinephrine induces pathway-specific long-lasting potentiation and depression in the hippocampal dentate gyrus. *Proceedings of the National Academy of Sciences, 86*(12), 4776-4780. https://doi.org/10.1073/pnas.86.12.4776

Del Tredici, K., & Braak, H. (2013). Dysfunction of the locus coeruleus-norepinephrine system and related circuitry in Parkinson's disease-related dementia. *J Neurol Neurosurg Psychiatry, 84*(7), 774-783. https://doi.org/10.1136/jnnp-2011-301817

Divac, I., Wikmark, R. G. E., & Gade, A. (1975). Behavioural changes after ablation of subdivisions of the rat prefrontal cortex. *Acta neurobiologiae experimentalis, 53*(3), 439-449.

Duka, V., Lee, J.-H., Credle, J., Wills, J., Oaks, A., Smolinsky, C., Shah, K., Mash, D. C., Masliah, E., Sidhu, A., & Reddy, H. (2013). Identification of the sites of tau hyperphosphorylation and activation of tau kinases in synucleinopathies and Alzheimer's diseases. *PLoS One, 8*(9), 1-11. https://doi.org/10.1371/journal.pone.0075025

Ehninger, D., & Kempermann, G. (2007). Neurogenesis in the adult hippocampus. *Cell and Tissue Research, 331*(1), 243-250. https://doi.org/10.1007/s00441-007-0478-3

Ennaceur, A., Neave, N., & Aggleton, J. P. (1996). Neurotoxic lesions of the perirhinal cortex do not mimic the behavioural effects of fornix transection in the rat. *Behavioural Brain Research, 80*(1-2), 9-25. https://doi.org/10.1016/0166-4328(96)00006-x

Folke, J., Pakkenberg, B., & Brudek, T. (2018). Impaired wnt signaling in the prefrontal cortex of Alzheimer's disease. *Molecular Neurobiology, 56*(2), 873-891. https://doi.org/10.1007/s12035-018-1103-z

Foote, S. L., Bloom, F. E., & Aston-Jones, G. (1983). Nucleus locus ceruleus: new evidence of anatomical and physiological specificity. *Physiological reviews, 63*(3), 844-914. https://doi.org/10.1152/physrev.1983.63.3.844

Galeano, P., Martino Adami, P. V., Do Carmo, S., Blanco, E., Rotondaro, C., Capani, F., Castaño, E. M., Cuello, A. C., & Morelli, L. (2014). Longitudinal analysis of the behavioral phenotype in a novel transgenic rat model of early stages of Alzheimer's disease. *Frontiers in Behavioral Neuroscience, 8*, 321-321. https://doi.org/10.3389/fnbeh.2014.00321

Ghosh, A., Torraville, S. E., Mukherjee, B., Walling, S. G., Martin, G. M., Harley, C. W., & Yuan, Q. (2019). An experimental model of Braak's pretangle proposal for the origin of Alzheimer's disease: the role of locus coeruleus in early symptom development. *Alzheimer's Research & Therapy, 11*(1), 59-59. https://doi.org/10.1186/s13195-019-0511-2

Gompf, H. S., Budygin, E. A., Fuller, P. M., & Bass, C. E. (2015). Targeted genetic manipulations of neuronal subtypes using promoter-specific combinatorial AAVs in wild-type animals. *Frontiers in Behavioral Neuroscience, 9*, 1-12. https://doi.org/10.3389/fnbeh.2015.00152

Hansen, N., & Manahan-Vaughan, D. (2015). Locus coeruleus stimulation facilitates long-term depression in the dentate gyrus that requires activation of β-adrenergic receptors. *Cerebral Cortex, 25*(7), 1889-1896. https://doi.org/10.1093/cercor/bht429

Harkany, T., Dijkstra, I. M., Oosterink, B. J., Horvath, K. M., Abraham, I., Keijser, J., Van der Zee, E. A., & Luiten, P. G. (2000). Increase amyloid precursor protein expression and serotonergic sprouting following excitotoxic lesion of the rat magnocellular nucleus basalis: neuroprotection by Ca^{2+} antagonist nimodipine. *Neuroscience, 101*(1), 101-114. https://doi.org/10.1016/S0306-4522(00)00296-7

Hoover, B. R., Reed, M. N., Su, J., Penrod, R. D., Kotilinek, L. A., Grant, M. K., Pitstick, R., Carlson, G. A., Lanier, L. M., Yuan, L.-L., Ashe, K. H., & Liao, D. (2010). Tau mislocalization to dendritic spines mediates synaptic dysfunction independently of neurodegeneration. *Neuron, 68*(6), 1067-1081. https://doi.org/10.1016/j.neuron.2010.11.030

Hou, L., Sun, F., Sun, W., Zhang, L., & Wang, Q. (2019). Lesion of the locus coeruleus damages learning and memory performance in paraquat and maneb-induced mouse Parkinson's disease model. *Neuroscience, 419*, 129-140. https://doi.org/10.1016/j.neuroscience.2019.09.006

Hu, Y. Y., He, S. S., Wang, X., Duan, Q. H., Grundke-Iqbal, I., Iqbal, K., & Wang, J. (2002). Levels of nonphosphorylated and phosphorylated tau in cerebrospinal fluid of Alzheimer's disease patients: an ultrasensitive bienzyme-substrate-recycle enzyme-linked immunosorbent assay. *American Journal of Pathology, 160*(4), 1269-1278. https://doi.org/10.1016/S0002-9440(10)62554-0

Hubert, M.-F., Laroque, P., Gillet, J.-P., & Keenan, K. P. (2000). The effects of diet, ad libitum feeding, and moderate and severe dietary restriction on body weight, survival, clinical pathology parameters, and cause of death in control Sprague-Dawley rats. *Toxicological Sciences, 58*(1), 195-207. https://doi.org/10.1093/toxsci/58.1.195

Hughes, R. N. (2004). The value of spontaneous alternation behavior (SAB) as a test of retention in pharmacological investigations of memory. *Neuroscience and Biobehavioral Reviews, 28*(5), 497-505. https://doi.org/10.1016/j.neubiorev.2004.06.006

Hyman, B. T., Phelps, C. H., Beach, T. G., Bigio, E. H., Cairns, N. J., Carrillo, M. C., Dickson, D. W., Duyckaerts, C., Frosch, M. P., Masliah, E., Mirra, S. S., Nelson, P. T., Schneider, J. A., Thal, D. R., Thies, B., Trojanowski, J. Q., Vinters, H. V., & Montine, T. J. (2012). National Institute on Aging-Alzheimer's Association guidelines for the neuropathologic assessment of Alzheimer's disease. *Alzheimer's & Dementia, 8*(1), 1-13. https://doi.org/10.1016/j.jalz.2011.10.007

Hyman, B. T., Van Hoesen, G. W., Kromer, L. J., & Damasio, A. R. (1986). Perforant pathway changes and the memory impairment of Alzheimer's disease. *Annals of Neurology, 20*(4), 472-481. https://doi.org/10.1002/ana.410200406

Iqbal, K., Zaidi, T., Wen, G. Y., Grundke-Iqbal, I., Merz, P. A., Shaikh, S. S., Wisniewski, H. M., AlafuzofT, I., & Winblad, B. (1987). Defective brain microtubule assembly in Alzheimer's disease. *Alzheimer Disease and Associated Disorders, 1*(3), 201-202. https://doi.org/10.1097/00002093-198701030-00017

Kelly, S. C., He, B., Perez, S. E., Ginsberg, S. D., Mufson, E. J., & Counts, S. E. (2017). Locus coeruleus cellular and molecular pathology during the progression of Alzheimer's disease. *Acta Neuropathologica Communications, 5*(1), 1-14. https://doi.org/10.1186/s40478-017-0411-2

Kelly, S. C., McKay, E. C., Beck, J. S., Collier, T. J., Dorrance, A. M., & Counts, S. E. (2019). Locus coeruleus degeneration induces forebrain vascular pathology in a transgenic rat model of Alzheimer's disease. *Journal of Alzheimer's Disease, 70*(2), 371-388. https://doi.org/10.3233/JAD-190090

Kempermann, G., Kuhn, H. G., & Gage, F. H. (1997). More hippocampal neurons in adult mice living in an enriched environment. *Nature, 386*(6624), 493-495. https://doi.org/10.1038/386493a0

Kingston, A., Comas-Herrera, A., & Jagger, C. (2018). Forecasting the care needs of the older population in England over the next 20 years: estimates from the Population Ageing and Care Simulation (PACSim) modelling study. *The Lancet. Public Health, 3*(9), e447-e455. https://doi.org/10.1016/s2468-2667(18)30118-x

Kitchigina, V., Vankov, A., Harley, C., & Sara, S. J. (1997). Novelty-elicited, noradrenaline-dependent enhancement of excitability in the dentate gyrus. *The European Journal of Neuroscience, 9*(1), 41-47. https://doi.org/10.1111/j.1460-9568.1997.tb01351.x

Kneynsberg, A., Combs, B., Christensen, K., Morfini, G., & Kanaan, N. M. (2017). Axonal degeneration in tauopathies: disease relevance and underlying mechanisms. *Frontiers in Neuroscience, 11*, 1-14. https://doi.org/10.3389/fnins.2017.00572

Kuhn, H. G., Dickinson-Anson, H., & Gage, F. H. (1996). Neurogenesis in the dentate gyrus of the adult rat: age-related decrease of neuronal progenitor proliferation. *The Journal of Neuroscience, 16*(6), 2027-2033. https://doi.org/10.1523/jneurosci.16-06-02027.1996

Kvetnansky, R., Sabban, E. L., & Palkovits, M. (2009). Catecholaminergic systems in stress: structural and molecular genetic approaches. *Physiological Reviews, 89*(2), 535-606. https://doi.org/10.1152/physrev.00042.2006

Lacaille, J.-C., & Harley, C. W. (1985). The action of norepinephrine in the dentate gyrus: Beta-mediated facilitation of evoked potentials in vitro. *Brain Research, 358*(1-2), 210-220. https://doi.org/10.1016/0006-8993(85)90965-5

Lemon, N., Aydin-Abidin, S., Funke, K., & Manahan-Vaughan, D. (2009). Locus coeruleus activation facilitates memory encoding and induces hippocampal LTD that depends on β-adrenergic receptor activation. *Cerebral Cortex, 19*(12), 2827-2837. https://doi.org/10.1093/cercor/bhp065

Lerchner, W., Corgiat, B., Der Minassian, V., Saunders, R. C., & Richmond, B. J. (2014). Injection parameters and virus dependent choice of promoters to improve neuron targeting in the nonhuman primate brain. *Gene Therapy, 21*(3), 233-241. https://doi.org/10.1038/gt.2013.75

Lethbridge, R. L., Walling, S. G., & Harley, C. W. (2014). Modulation of the perforant path-evoked potential in dentate gyrus as a function of intrahippocampal β-adrenoceptor agonist concentration in urethane-anesthetized rat. *Brain and Behavior, 4*(1), 95-103. https://doi.org/10.1002/brb3.199

Lindvall, O., & Bjorklund, A. (1974). The organization of the ascending catecholamine neuron systems in the rat brain. As revealed by the glyoxylic acid fluorescence method. *Acta Physiologica Scandinavica, 92*(412),1-48.

Loughlin, S. E., Foote, S. L., & Grzanna, R. (1986). Efferent projections of nucleus locus coeruleus: Morphologic subpopulations have different efferent targets. *Neuroscience, 18*(2), 307-319. https://doi.org/10.1016/0306-4522(86)90156-9

Mason, S. T., & Fibiger, H. C. (1979). Regional topography within noradrenergic locus coeruleus as revealed by retrograde transport of horseradish peroxidase. *Journal of Comparative Neurology, 187*(4), 703-724. https://doi.org/10.1002/cne.901870405

Mather, M., Clewett, D., Sakaki, M., & Harley, C. W. (2016). Norepinephrine ignites local hot spots of neuronal excitation: How arousal amplifies selectivity in perception and memory. *The Behavioral and Brain Sciences, 39*, 1-75. https://doi.org/10.1017/S0140525X15000667

McDonald, R. J., & White, N. M. (1995). Hippocampal and nonhippocampal contributions to place learning in rats. *Behavioral Neuroscience, 109*(4), 579-593. https://doi.org/10.1037/0735-7044.109.4.579

McKeever, P. M., Schneider, R., Taghdiri, F., Weichert, A., Multani, N., Brown, R. A., Boxer, A. L., Karydas, A., Miller, B., Robertson, J., & Tartaglia, M. C. (2018). MicroRNA expression levels are altered in the cerebrospinal fluid of patients with young-onset Alzheimer's disease. *Molecular Neurobiology, 55*(12), 8826-8841. https://doi.org/10.1007/s12035-018-1032-x

Means, L. W., David Leander, J., & Isaacson, R. L. (1971). The effects of hippocampectomy on alternation behavior and response to novelty. *Physiology & Behavior, 6*(1), 17-22. https://doi.org/10.1016/0031-9384(71)90006-0

Méndez-López, M., Méndez, M., López, L., & Arias, J. L. (2009). Spatial working memory in Wistar rats: Brain sex differences in metabolic activity. *Brain Research Bulletin, 79*(3), 187-192. https://doi.org/10.1016/j.brainresbull.2009.02.007

Mogensen, J., & Divac, I. (1993). Behavioural changes after ablation of subdivisions of the rat prefrontal cortex. *Acta Neurobiologiae Experimentalis, 53*(3), 439-449.

Moore, R. Y., & Bloom, F. E. (1978). Central catecholamine neuron systems: anatomy and physiology of the dopamine systems. *Annual Review of Neuroscience, 1*(1), 129-169. https://doi.org/10.1146/annurev.ne.01.030178.001021

Mumby, D. G., & Pinel, J. P. J. (1994). Rhinal cortex lesions and object recognition in rats. *Behavioral Neuroscience, 108*(1), 11-18. https://doi.org/10.1037/0735-7044.108.1.11

Neuman, K. M., Molina-Campos, E., Musial, T. F., Price, A. L., Oh, K.-J., Wolke, M. L., Buss, E. W., Scheff, S. W., Mufson, E. J., & Nicholson, D. A. (2015). Evidence for Alzheimer's disease-linked synapse loss and compensation in mouse and human hippocampal CA1 pyramidal neurons. *Brain Structure and Function, 220*(6), 3143-3165. https://doi.org/10.1007/s00429-014-0848-z

Neuman, R. S., & Harley, C. W. (1983). Long-lasting potentiation of the dentate gyrus population spike by norepinephrine. *Brain Research, 273*(1), 162-165. https://doi.org/10.1016/0006-8993(83)91106-X

O'Donnell, J., Zeppenfeld, D., McConnell, E., Pena, S., & Nedergaard, M. (2012). Norepinephrine: A neuromodulator that boosts the function of multiple cell types to optimize CNS performance. *Neurochemical Research, 37*(11), 2496-2512. https://doi.org/10.1007/s11064-012-0818-x

Okamoto, M., Inoue, K., Iwamura, H., Terashima, K., Soya, H., Asashima, M., & Kuwabara, T. (2011). Reduction in paracrine wnt3 factors during aging causes impaired adult neurogenesis. *The FASEB Journal, 25*(10), 3570-3582. https://doi.org/10.1096/fj.11-184697

Ortiz-Mamamoros, A., Salcedo-Tello, P., Avila-Munoz, E., Zepeda, A., & Arias, C. (2013). Role of wnt signaling in the control of adult hippocampal functioning in health and disease: Therapeutic implications. *Current Neuropharmacology, 11*(5), 465-476. https://doi.org/10.2174/1570159x11311050001

Paxinos, G., & Watson, C. (2007). *The rat brain in stereotaxic coordinates* (Compact 6th ed.). Elsevier Academic.

Perry, R. J. (1999). Attention and executive deficits in Alzheimer's disease: A critical review. *Brain, 122*(3), 383-404. https://doi.org/10.1093/brain/122.3.383

Phinney, A. L., Deller, T., Stalder, M., Calhoun, M. E., Frotscher, M., Sommer, B., Staufenbiel, M., & Jucker, M. (1999). Cerebral amyloid induces abberant axonal sprouting and ectopic terminal formation in amyloid precursor protein transgenic mice. *Journal of Neuroscience, 19* (19), 8552-8559. https://doi.org/10.1523/JNEUROSCI.19-19-08552.1999

Quinlan, M. A. L., Strong, V. M., Skinner, D. M., Martin, G. M., Harley, C. W., & Walling, S. G. (2019). Locus coeruleus optogenetic light activation induces long-term potentiation of perforant path population spike amplitude in rat dentate Gyrus. *Frontiers in Systems Neuroscience, 12*, 1-14. https://doi.org/10.3389/fnsys.2018.00067

Ramirez, J. J., & Stein, D. G. (1984). Sparing and recovery of spatial alternation performance after entorhinal cortex lesions in rats. *Behavioural Brain Research, 13*(1), 53-61. https://doi.org/10.1016/0166-4328(84)90029-9

Reiman, E. M. (2016). Alzheimer's disease: Attack on amyloid-β protein. *Nature, 537*(7618), 36-37. https://doi.org/10.1038/537036a

Rorabaugh, J. M., Chalermpalanupap, T., Botz-Zapp, C. A., Fu, V. M., Lembeck, N. A., Cohen, R. M., & Weinshenker, D. (2017). Chemogenetic locus coeruleus activation restores reversal learning in a rat model of Alzheimer's disease. *Brain, 140*(11), 3023-3038. https://doi.org/10.1093/brain/awx232

Ross, J. A., Reyes, B. A. S., & Van Bockstaele, E. J. (2019). Amyloid beta peptides, locus coeruleus-norepinephrine system and dense core vesicles. *Brain Research, 1702*, 46-53. https://doi.org/10.1016/j.brainres.2018.03.009

Sato, N., Meijer, L., Skaltsounis, L., Greengard, P., & Brivanlou, A. H. (2003). Maintenance of pluripotency in human and mouse embryonic stem cells through activation of wnt signaling by a pharmacological GSK-3-specific inhibitor. *Nature Medicine, 10*(1), 55-63. https://doi.org/10.1038/nm979

Satoh, K., Tohyama, M., Yamamoto, K., Sakumoto, T., & Shimizu, N. (1977). Noradrenaline innervation of the spinal cord studied by the horseradish peroxidase method combined with monoamine oxidase staining. *Experimental Brain Research, 30*(2-3), 175-186. https://doi.org/10.1007/BF00237249

Scheltens, P., Blennow, K., Breteler, M., de Strooper, B., Frisoni, G., & Salloway, S. (2016). Alzheimer's disease. *Lancet, 388*(10043), 505-517. https://doi.org/10.1016/S0140-6736(15)01124-1

Sengupta, U., Nilson, A. N., & Kayed, R. (2016). The role of amyloid-β oligomers in toxicity, propagation, and immunotherapy. *EBioMedicine, 6*, 42-49. https://doi.org/10.1016/j.ebiom.2016.03.035

Shakhawat, A. M. D., Gheidi, A., MacIntyre, I. T., Walsh, M. L., Harley, C. W., & Yuan, Q. (2015). Arc-expressing neuronal ensembles supporting pattern separation require adrenergic activity in anterior piriform cortex: An exploration of neural constraints on learning. *The Journal of Neuroscience, 35*(41), 14070-14075. https://doi.org/10.1523/JNEUROSCI.2690-15.2015

Sivanandam, T. M., & Thakur, M. K. (2012). Traumatic brain injury: a risk factor for Alzheimer's disease. *Neuroscience and Biobehavioral Reviews, 36*(5), 1376-1381. https://doi.org/10.1016/j.neubiorev.2012.02.013

Small, S. A., Schobel, S. A., Buxton, R. B., Witter, M. P., & Barnes, C. A. (2011). A pathophysiological framework of hippocampal dysfunction in ageing and disease. *Nature Reviews. Neuroscience, 12*(10), 585-601. https://doi.org/10.1038/nrn3085

Stevens, L., Vonck, K., Larsen, L. E., Van Lysebettens, W., Germonpré, C., Baekelandt, V., Van den Haute, C., Carrette, E., Wadman, W. J., Boon, P., & Raedt, R. (2020). A feasibility study to investigate chemogenetic modulation of the locus coeruleus by means of single unit activity. *Frontiers in Neuroscience, 14*, 1-9. https://doi.org/10.3389/fnins.2020.00162

Stevens, R., & Cowey, A. (1973). Effects of dorsal and ventral hippocampal lesions on spontaneous alternation, learned alternation and probability learning in rats. *Brain Research, 52*, 203-224. https://doi.org/10.1016/0006-8993(73)90659-8

Swanson, L. W., & Hartman, B. K. (1975). The central adrenergic system. An immunofluorescence study of the location of cell bodies and their efferent connections in the rat utilizing dopamine-B-hydroxylase as a marker. *Journal of Comparative Neurology (1911), 163*(4), 467-505. https://doi.org/10.1002/cne.901630406

Tomlinson, B. E., Irving, D., & Blessed, G. (1981). Cell loss in the locus coeruleus in senile dementia of Alzheimer type. *Journal of the Neurological Sciences, 49*(3), 419-428. https://doi.org/10.1016/0022-510X(81)90031-9

Tsien, J. Z., Huerta, P. T., &Tonegawa, S. (1996). The essential role of hippocampal CA1 NMDA receptor-dependent synaptic plasticity in spatial memory. *Cell, 87*(7), 1327-1338. https://doi.org/10.1016/s0092-8674(00)81827-9

Vazey, E., M., & Aston-Jones, G. (2014). Designer receptor manipulations reveal a role of the locus coeruleus noradrenergic system in isoflurane general anesthesia. *Proceedings of the National Academy of Sciences, 111*(10), 3859-3864. https://doi.org/10.1073/pnas.1310025111

Walling, S. G., & Harley, C. W. (2004). Locus ceruleus activation initiates delayed synaptic potentiation of perforant path input to the dentate gyrus in awake rats: a novel beta-adrenergic- and protein synthesis-dependent mammalian plasticity mechanism. *The Journal of Neuroscience, 24*(3), 598-604. https://doi.org/10.1523/JNEUROSCI.4426-03.2004

Walling, S. G., Milway, J. S., Ingram, M., Lau, C., Morrison, G., & Martin, G. M. (2016). The effects of prolonged administration of norepinephrine reuptake inhibitors on long-term potentiation in dentate gyrus, and on tests of spatial and object recognition memory in rats. *Neurobiology of Learning and Memory, 128*, 92-102. https://doi.org/10.1016/j.nlm.2015.12.013

Walling, S. G., Nutt, D. J., Lalies, M. D., & Harley, C. W. (2004). Orexin-A infusion in the locus ceruleus triggers norepinephrine (NE) release and NE-induced long-term potentiation in the dentate gyrus. *The Journal of Neuroscience, 24*(34), 7421-7426. https://doi.org/10.1523/jneurosci.1587-04.2004

Weinshenker, D. (2008). Functional consequences of locus coeruleus degeneration in Alzheimer's disease. *Current Alzheimer Research, 5*(3), 342-345. https://doi.org/10.2174/156720508784533286

Winters, B. D., & Bussey, T. J. (2005). Transient inactivation of perirhinal cortex disrupts encoding, retrieval, and consolidation of object recognition memory. *Journal of Neuroscience, 25*(1), 52-61. https://doi.org/10.1523/JNEUROSCI.3827-04.2005

Wu, Y.-T., Fratiglioni, L., Matthews, F. E., Lobo, A., Breteler, M. M. B., Skoog, I., & Brayne, C. (2016). Dementia in western Europe: epidemiological evidence and implications for policy making. *Lancet Neurology, 15*(1), 116-124. https://doi.org/10.1016/S1474-4422(15)00092-7

Xu, J., & Zhu, Y. (2018). A rapid in vitro method to flip back the double-floxed inverted open reading frame in a plasmid. *BMC biotechnology, 18*(1), 1-12. https://doi.org/10.1186/s12896-018-0462-x

Xu, W., Yu, J.-T., Tan, M.-S., & Tan, L. (2014). Cognitive reserve and Alzheimer's disease. *Molecular Neurobiology, 51*(1), 187-208. https://doi.org/10.1007/s12035-014-8720-y

Yeckel, M. F., & Berger, T. W. (1990). Feedforward excitation of the hippocampus by afferents from the entorhinal cortex: redefinition of the role of the trisynaptic pathway. *Proceedings of the National Academy of Sciences, 87*(15), 5832-5836. https://doi.org/10.1073/pnas.87.15.5832

Yiannopoulou, K. G., Anastasiou, A. I., Zachariou, V., & Pelidou, S.-H. (2019). Reasons for failed trials of disease-modifying treatments for Alzheimer disease and their contribution in recent research. *Biomedicines, 7*(4), 1-16. https://doi.org/10.3390/biomedicines7040097

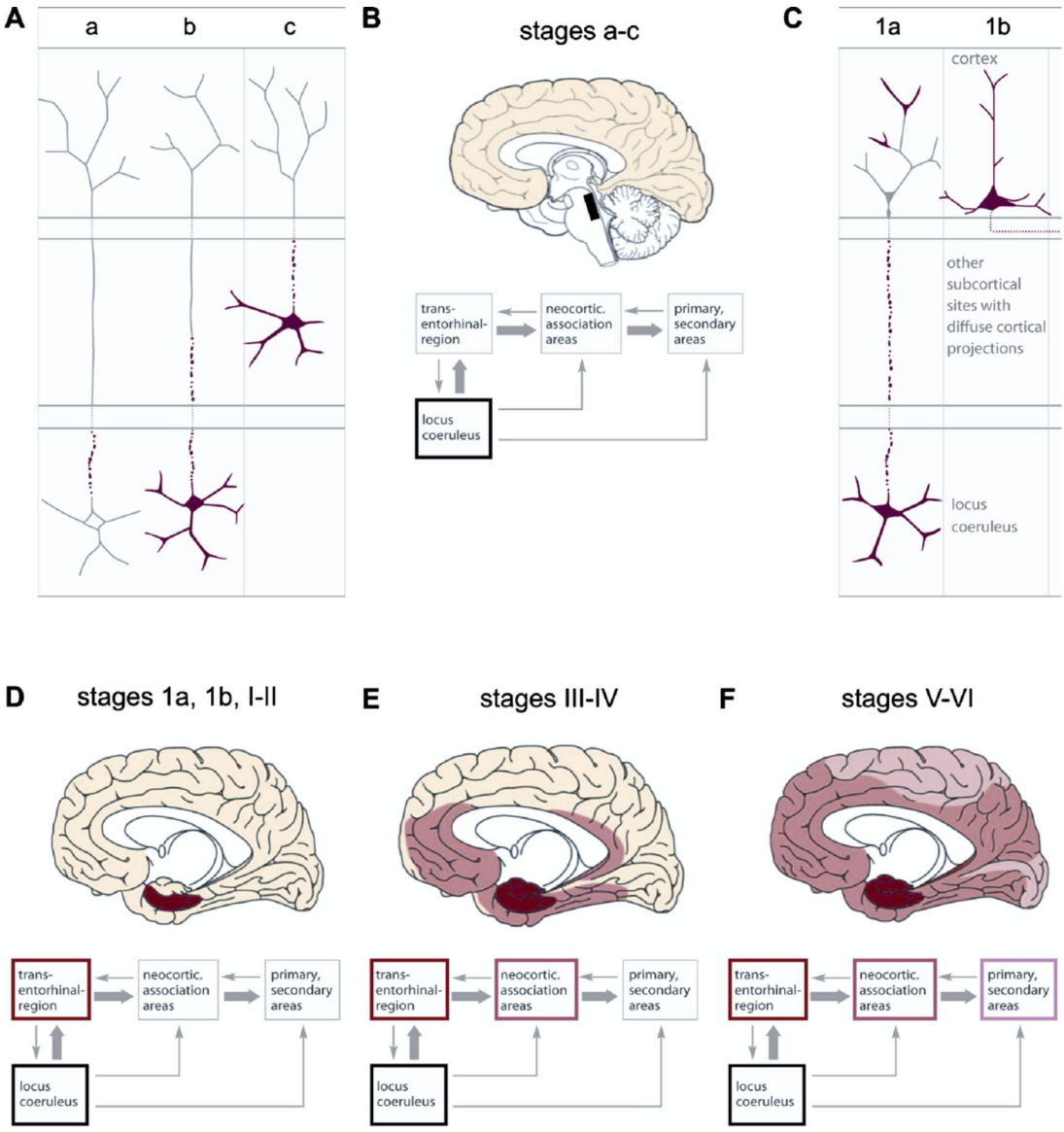

Figure 1. Stages of Alzheimer disease (AD)-associated tau pathology. Image adapted from Braak et al. (2011). **(A)** In stage a, cellular processes of locus coeruleus (LC) neurons accumulate pretangle material. Then, at stage b, this pretangle material fills the soma and dendrites. In stage c, this material is found in other thalamic brainstem nuclei. **(B)** A schematic representation of stages a-c. **(C)** In stage 1a, pretangle material begins to appear in the transentorhinal cortex. In stage 1b, the soma and cellular processes of

transentorhinal pyramidal cells are filled with pretangle material. **(D)** A schematic representation of stages 1a, 1b, I and II. **(E)** A schematic representation of stages III and IV. **(F)** A schematic representation of stages V and VI.

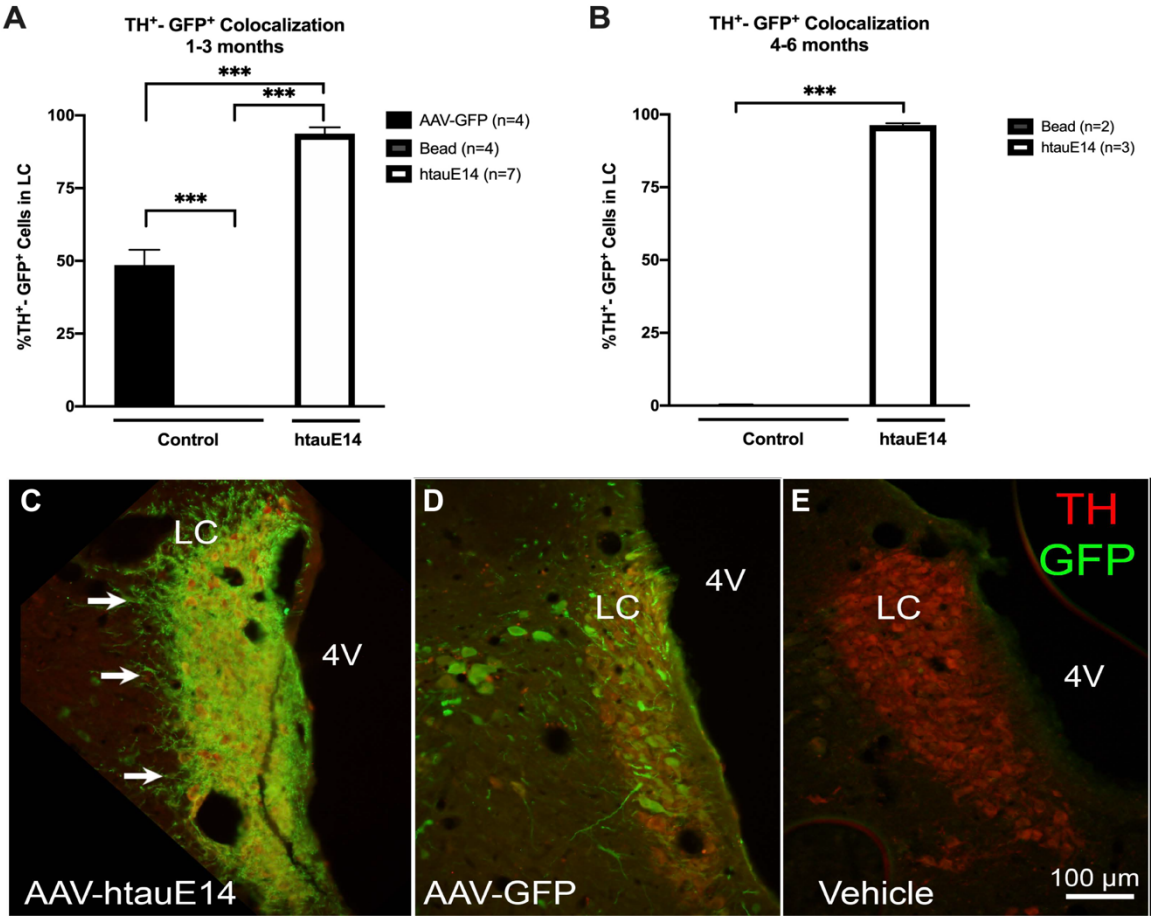

Figure 2. Colocalization of tyrosine hydroxylase-positive (TH^+) and green fluorescent protein-positive (GFP^+) locus coeruleus (LC) neurons. **(A)** Percentage of TH^+ - GFP^+ cells in the LC at 1-3 months p.i. in htauE14 and control animals. **(B)** Percentage of TH^+ - GFP^+ cells in the LC at 4-6 months p.i. in htauE14 and control animals. Digital images taken using an Olympus BX-52 microscope and DP72 digital camera show examples of an AAV-htauE14 **(C)**, AAV-GFP **(D)**, and non-viral infusion **(E)**. The arrows in panel **C** show the location of GPF in the neurites of LC neurons. All data represent means (+ SEM). *** $p < 0.001$. 4V = 4th ventricle.

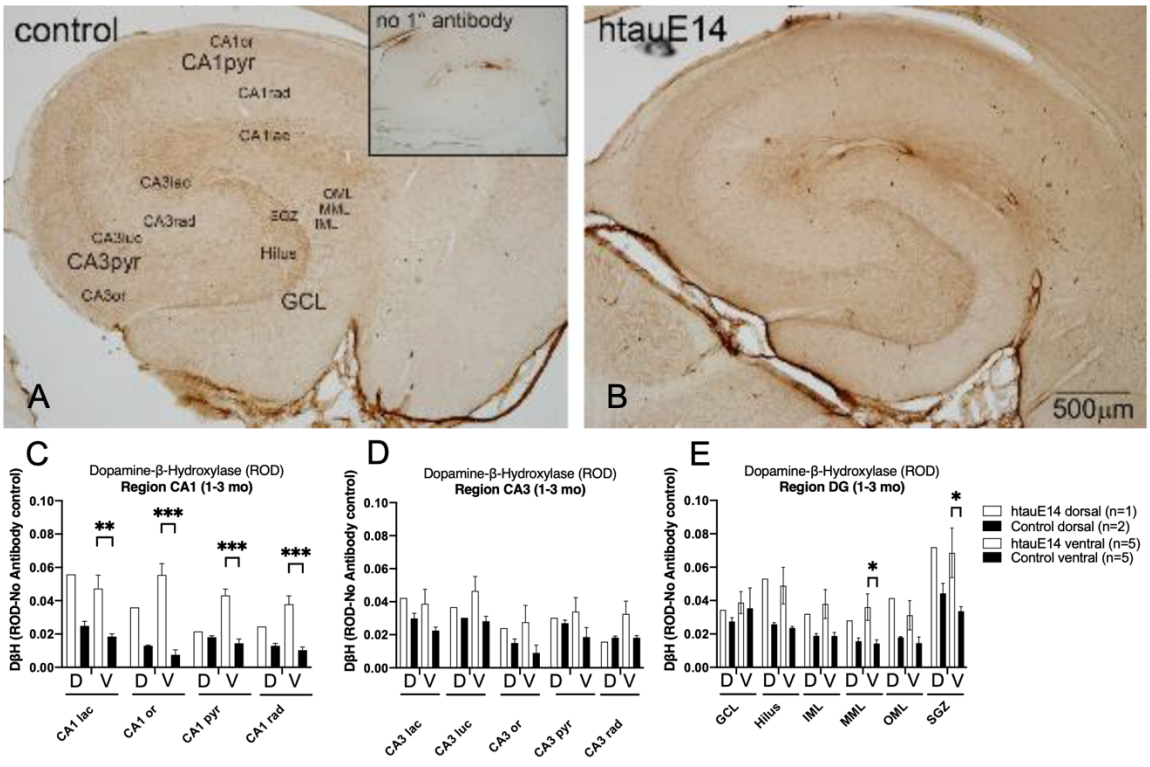

Figure 3. Brightfield images of DβH immunoreactivity in the hippocampus at a magnification of 4× for **(A)** control and **(B)** htauE14 animals and relative optical density graphs **(C-E)** for htauE14 and control animals at 1-3 months p.i., sexes combined, for three major regions of the hippocampus: cornu ammonis 1 (CA1), cornu ammonis 3 (CA3), and dentate gyrus (Lethbridge et al.). CA1 was divided into four subregions: CA1 lacunosum moleculare (CA1 lac), CA1 oriens (CA1 or), CA1 pyramidal (CA1 pyr), and CA1 radiatum (CA1 rad). CA3 was divided into five subregions: CA3 lacunosum moleculare (CA3 lac), CA3 lucidum (CA3 luc), CA3 oriens (CA3 or), CA3 pyramidal (CA3 pyr), and CA3 radiatum (CA3 rad). Dentate gyrus was divided into six subregions: granular cell layer (GCL), hilus, inner molecular layer (IML), middle molecular layer (MML), outer molecular layer, and subgranular zone (SGZ). The left-most graph **(C)** displays the data for the subregions of CA1, the middle graph **(D)** displays the data for the

subregions of CA3, and the right-most graphs **(E)** displays the data for the subregions of DG. All data represent means (+SEM). * $p < 0.05$. ** $p < 0.01$. *** $p < 0.001$. *Inset image:* Tissue section not treated with the primary antibody.

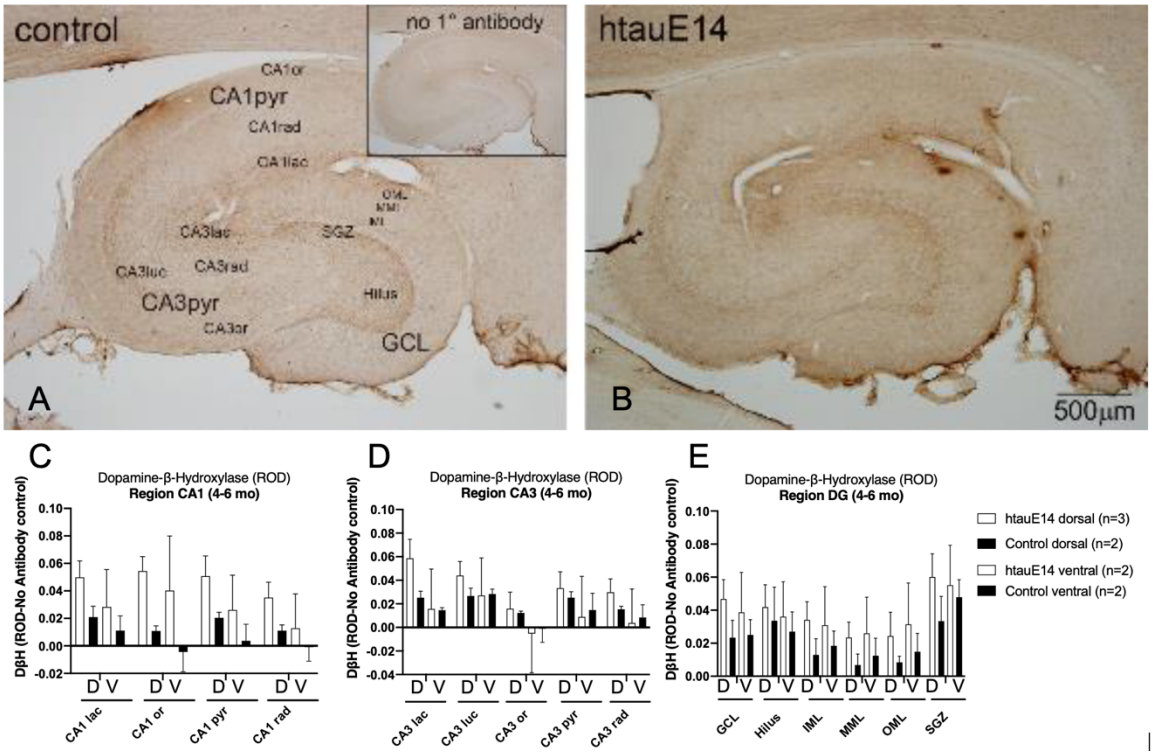

Figure 4. Brightfield images of DβH immunoreactivity in the hippocampus at a magnification of 4× for **(A)** control and **(B)** htauE14 animals and relative optical density graphs **(C-E)** for htauE14 and control animals at 4-6 months p.i., sexes combined, for three major regions of the hippocampus: cornu ammonis 1 (CA1), cornu ammonis 3 (CA3), and dentate gyrus (Lethbridge et al.). CA1 was divided into four subregions: CA1 lacunosum moleculare (CA1 lac), CA1 oriens (CA1 or), CA1 pyramidal (CA1 pyr), and CA1 radiatum (CA1 rad). CA3 was divided into five subregions: CA3 lacunosum moleculare (CA3 lac), CA3 lucidum (CA3 luc), CA3 oriens (CA3 or), CA3 pyramidal (CA3 pyr), and CA3 radiatum (CA3 rad). Dentate gyrus was divided into six subregions: granular cell layer (GCL), hilus, inner molecular layer (IML), middle molecular layer (MML), outer molecular layer, and subgranular zone (SGZ). The left-most graph **(C)** displays the data for the subregions of CA1, the middle graph **(D)** displays the data for the

subregions of CA3, and the right-most graphs **(E)** displays the data for the subregions of DG. All data represent means (+SEM). * $p < 0.05$. ** $p < 0.01$. *** $p < 0.001$. *Inset image:* Tissue section not treated with the primary antibody.

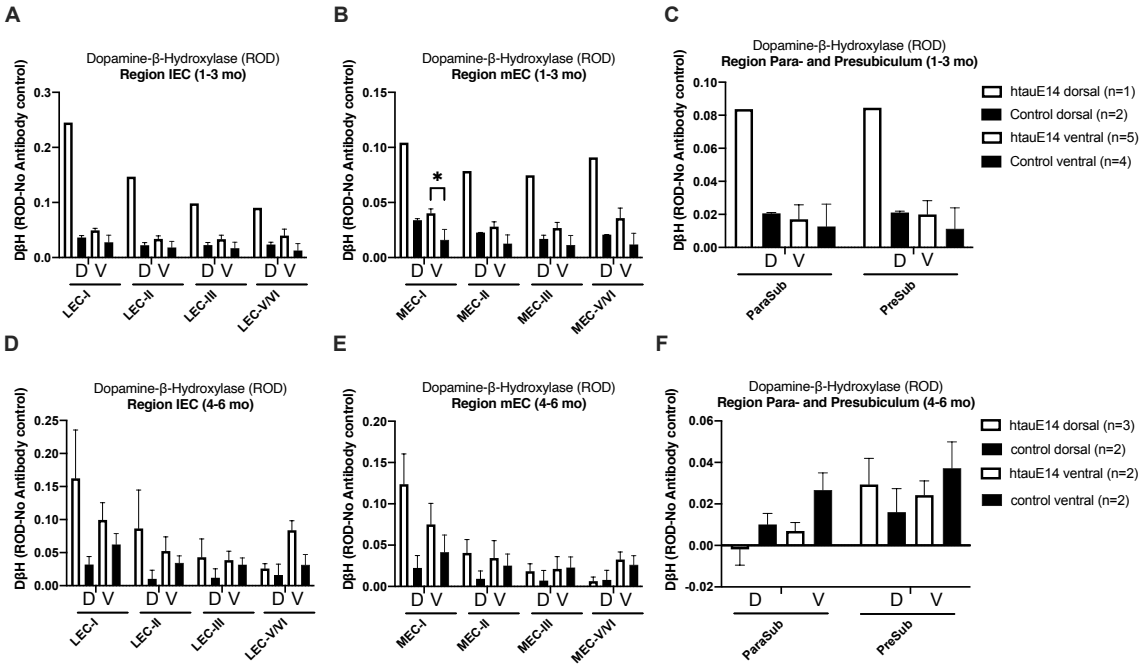

Figure 5. Relative optical density for htauE14 and control animals, sexes combined, at **(A-C)** 1-3 months and **(D-F)** 4-6 months p.i. for layers I to VI of the entorhinal cortex, the parasubiculum, and the presubiculum. The entorhinal cortex was divided into two regions: lateral entorhinal cortex (lEC) and medial entorhinal cortex (mEC). Both mEC and lEC were further divided into five layers. The subiculum was also divided into two regions: parasubiculum (ParaSub) and presubiculum (PreSub). The left-most graphs **(A, D)** display the data for the subregions of lEC, the middle graphs **(B, E)** display the data for the subregions of mEC, and the right-most graphs **(C, F)** display the data for the parasubiculum and the presubiculum. * $p < 0.05$

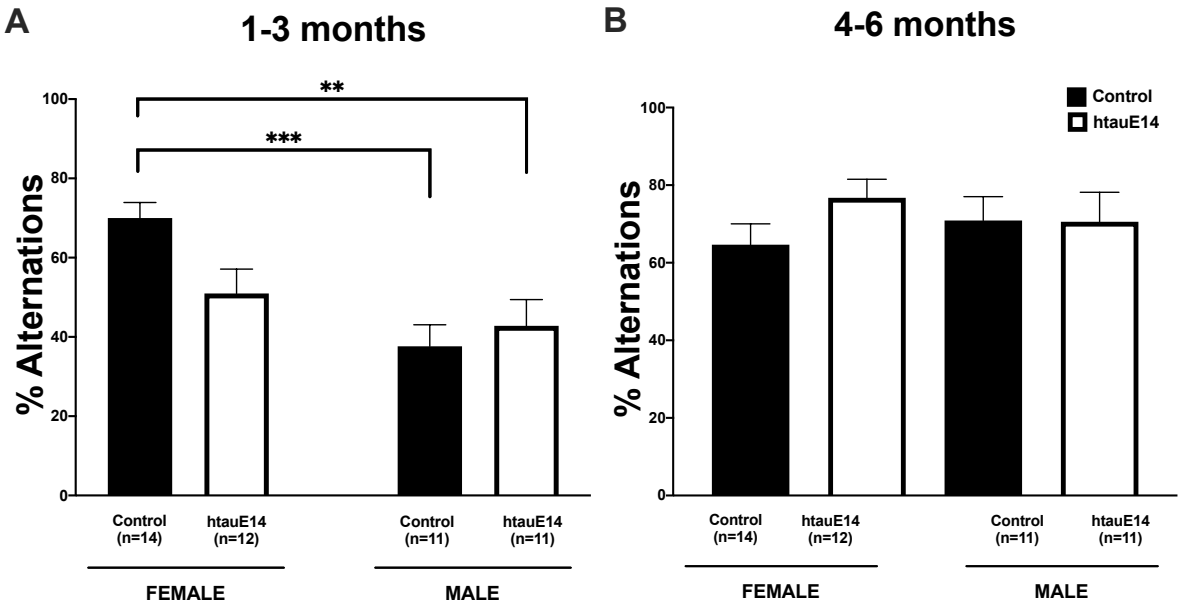

Figure 6. Percentage of alternations for the spontaneous alternation task at **(A)** 1-3 and **(B)** 4-6 months p.i. All data represent means (+SEM). ** $p < 0.01$. *** $p < 0.001$.

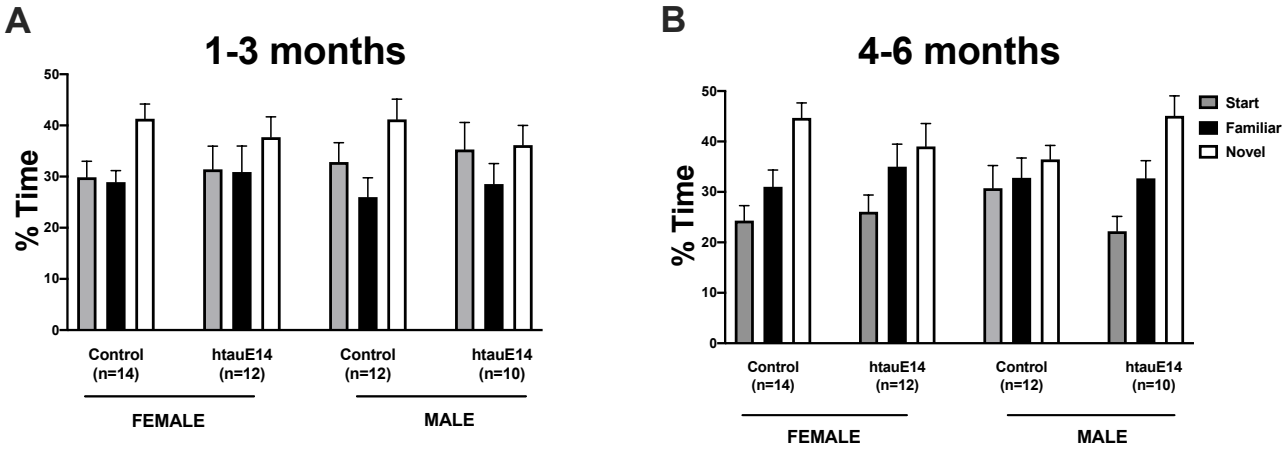

Figure 7. Percentage of time spent in arms (Start vs. Familiar vs. Novel) for the novel object recognition test at **(A)** 1-3 and **(B)** 4-6 months. All data represent means (+SEM).

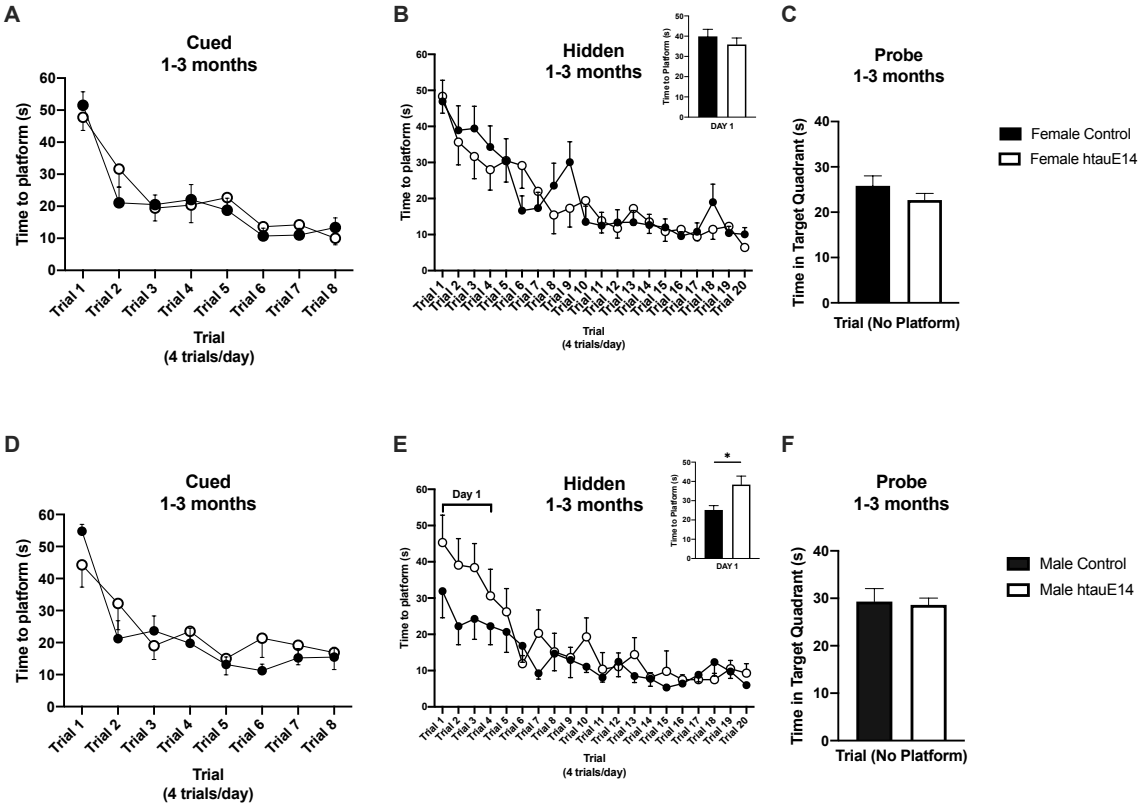

Figure 8. Behavioural data for three phases of the Morris water maze (MWM) task at 1-3 months p.i. Time to locate the flagged platform, in seconds, during the Cued phase of the task for **(A)** females and **(D)** males. Time to locate the hidden platform, in seconds, during the Hidden phase of the task for **(B)** females and **(E)** males. Time spent in the target quadrant, in seconds, during the Probe phase of the task for **(C)** females and **(F)** males. *Inset graph:* Average time to locate the platform, in seconds, on Day 1 of the hidden phase. All data represent means (±SEM). * $p < 0.05$.

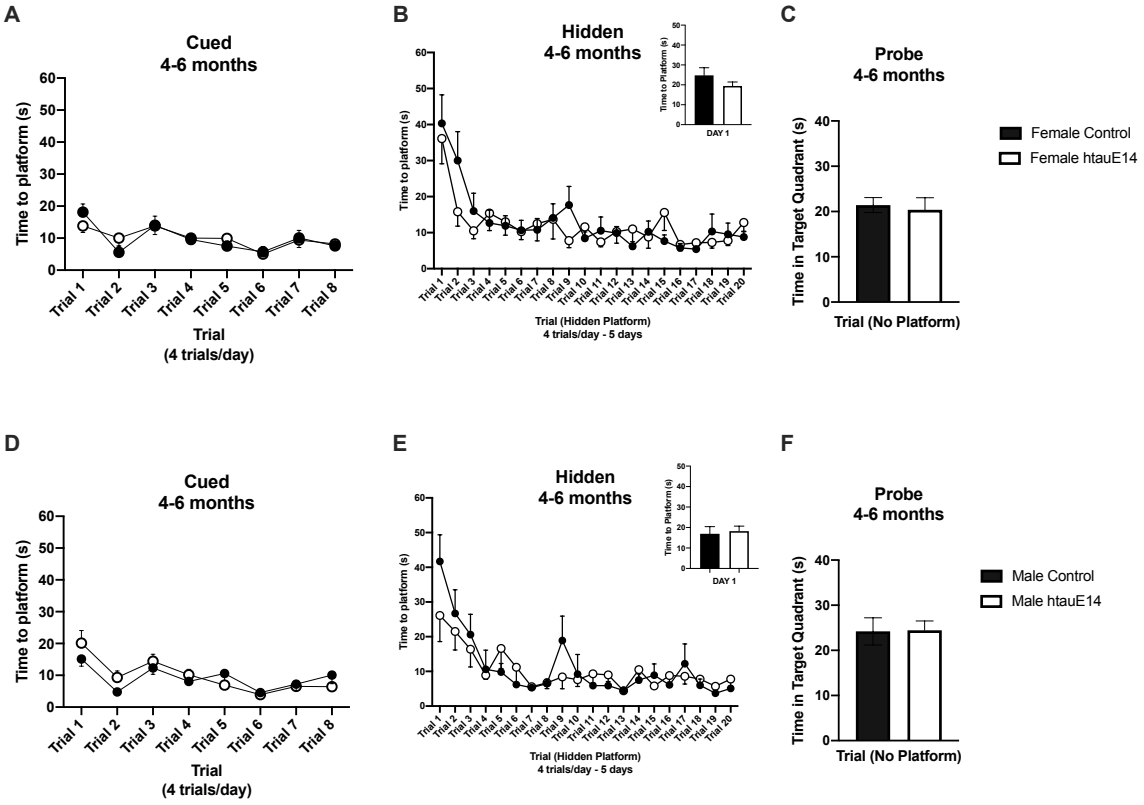

Figure 9. Behavioural data for three phases of the Morris water maze (MWM) task at 4-6 months p.i. Time to locate the flagged platform, in seconds, during the Cued phase of the task for **(A)** females and **(D)** males. Time to locate the hidden platform, in seconds, during the Hidden phase of the task for **(B)** females and **(E)** males. Time spent in the target quadrant, in seconds, during the Probe phase of the task for **(C)** females and **(F)** males. *Inset graph:* Average time to locate the platform, in seconds, on Day 1 of the hidden phase. All data represent means (±SEM).

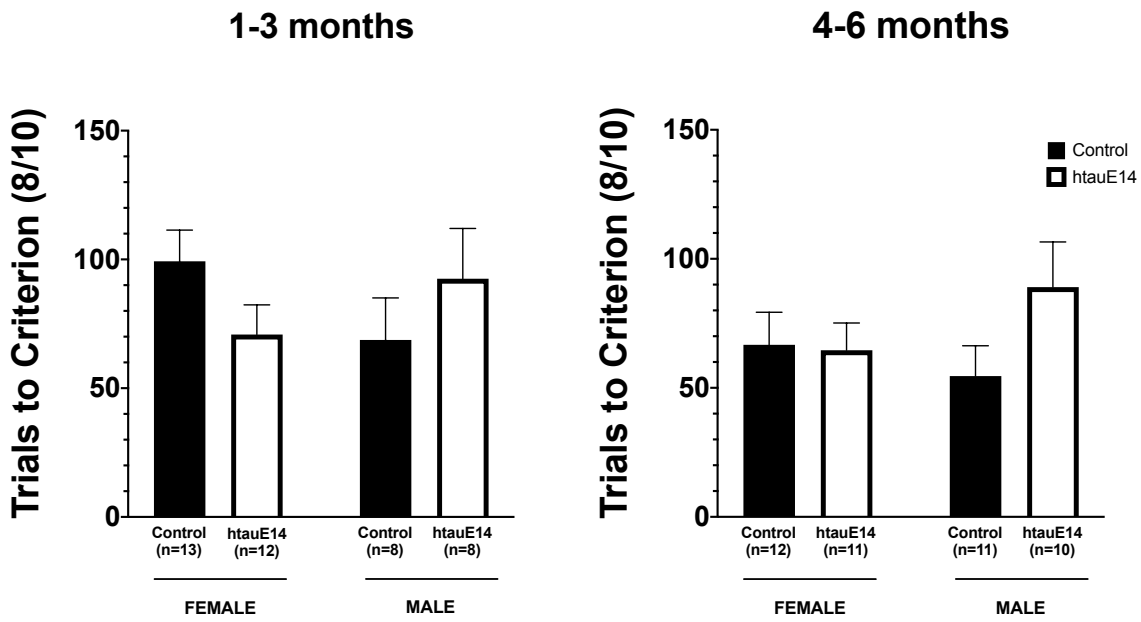

Figure 10. Trials to criterion (8/10) for the adjacent condition of the radial arm maze (RAM) task. All data represent means (+SEM).

Table 1

Number of samples taken, and cursor sizes used for densitometry analysis using MCID Analysis

Brain Region	Number of Samples	Cursor Diameter (Pixels)
Hippocampal complex		
Subgranular zone	25	15
Dentate gyrus	20	20
Hilus	15	20
Inner molecular layer	20	20
Middle molecular layer	20	20
Outer molecular layer	20	20
CA1 lacunosum moleculare	16	25
CA1 oriens	15	25
CA1 pyramidal	15	25
CA1 radiatum	18	25
CA3 lacunosum moleculare	12	25
CA3 lucidum	20	20
CA3 oriens	18	25
CA3 pyramidal	18	25
CA3 radiatum	18	25
Entorhinal cortex		

Medial entorhinal cortex		
Layer I	12 (6) *	25
Layer II	12	25
Layer III	18	25
Layer V-VI	15 (10) *	25
Lateral entorhinal cortex		
Layer I	6 (12) *	25
Layer II	12	25
Layer III	15	25
Layer V-VI	10 (15) *	25
Subiculum		
Parasubiculum	5	25
Preasubiculum	5	25

* The number of samples taken for some regions differed at varying dorsal-ventral levels of the brain. The numbers in brackets is the number of samples taken at ventral levels.